Geophysical Prospecting

EAGE EUROPEAN ASSOCIATION OF GEOSCIENTISTS & ENGINEERS

Geophysical Prospecting, 2016, **64**, 361–391 doi: 10.1111/1365-2478.12290

Unified multi-depth-level field decomposition

Niels Grobbe*, Joost van der Neut, Evert Slob, Kees Wapenaar, Carlos Almagro Vidal and Guy Drijkoningen

Department of Geoscience and Engineering, Section of Applied Geophysics and Petrophysics, Delft University of Technology, Stevinweg 1, 2628 CN Delft, The Netherlands

Received August 2014, revision accepted March 2015

ABSTRACT

Wavefield decomposition forms an important ingredient of various geophysical methods. An example of wavefield decomposition is the decomposition into upgoing and downgoing wavefields and simultaneous decomposition into different wave/field types. The multi-component field decomposition scheme makes use of the recordings of different field quantities (such as particle velocity and pressure). In practice, different recordings can be obscured by different sensor characteristics, requiring calibration with an unknown calibration factor. Not all field quantities required for multi-component field decomposition might be available, or they can suffer from different noise levels. The multi-depth-level decomposition approach makes use of field quantities recorded at multiple depth levels, e.g., two horizontal boreholes closely separated from each other, a combination of a single receiver array combined with free-surface boundary conditions, or acquisition geometries with a high-density of vertical boreholes. We theoretically describe the multi-depth-level decomposition approach in a unified form, showing that it can be applied to different kinds of fields in dissipative, inhomogeneous, anisotropic media, e.g., acoustic, electromagnetic, elastodynamic, poroelastic, and seismoelectric fields. We express the one-way fields at one depth level in terms of the observed fields at multiple depth levels, using extrapolation operators that are dependent on the medium parameters between the two depth levels. Lateral invariance at the depth level of decomposition allows us to carry out the multi-depth-level decomposition in the horizontal wavenumber–frequency domain. We illustrate the multi-depth-level decomposition scheme using two synthetic elastodynamic examples. The first example uses particle velocity recordings at two depth levels, whereas the second example combines recordings at one depth level with the Dirichlet free-surface boundary condition of zero traction. Comparison with multi-component decomposed fields shows a perfect match in both amplitude and phase for both cases. The multi-depth-level decomposition scheme is fully customizable to the desired acquisition geometry. The decomposition problem is in principle an inverse problem. Notches may occur at certain frequencies, causing the multi-depth-level composition matrix to become uninvertible, requiring additional notch filters. We can add multi-depth-level free-surface boundary conditions as extra equations to the multi-component composition matrix, thereby overdetermining this inverse problem. The combined multi-component–multi-depth-level decomposition on a land data set clearly shows improvements in the decomposition results, compared with the performance of the multi-component decomposition scheme.

*E-mail: ngrobbe@gmail.com

INTRODUCTION

Separation of recorded fields into downgoing and upgoing constituents is a technique that is used in many geophysical methods. Decomposed fields form the basis for various surface-related multiple elimination and deghosting procedures (e.g., Frijlink, Van Borselen, and Söellner 2011; Majdanski *et al.* 2011) and for depth imaging using primary and multiple reflections (e.g., Muijs, Robertsson, and Holliger 2007). Novel methodologies that make use of horizontal downhole sensors, such as the virtual source method (e.g., Bakulin and Calvert 2006; Mehta *et al.* 2007; Alexandrov, Bakulin, and Burnstad 2012) and multi-dimensional deconvolution Wapenaar *et al.* 2011, rely on decomposing the seismic field at depth.

The principle of decomposition can be applied to all kinds of fields. However, applying field decomposition to a real data set is often quite challenging. The multi-component (MC) field decomposition scheme makes use of differently recorded field components, e.g., both pressure (p) and vertical component particle velocity (v_3) data for a purely acoustic case (e.g., White 1965; Day *et al.* 2013).

In practice, recordings can be obscured by different sensor characteristics, requiring calibration with an unknown calibration factor (e.g., Schalkwijk, Wapenaar, and Verschuur 2003; Day *et al.* 2013). A way to find the calibration factor for land data with buried receivers was described by Alexandrov *et al.* (2014). They make use of auto-correlations and cross-correlations between the geophone and hydrophone data (with muted direct arrivals) and find the calibration factor by minimizing the auto-correlation energy in a time window placed around an estimated two-way travel time. In addition to the problem of an unknown calibration factor, the noise levels might be different for different sensor types, resulting in different data quality for different fields (Burnstad *et al.* 2012). This can lead to unsatisfactory decomposed data. Furthermore, not all field quantities required for MC field decomposition might be available. Especially, when dealing with more complex field phenomena (e.g., elastodynamic or seismoelectric fields), the MC field decomposition requires measuring many different field quantities. Let us focus for example on the elastodynamic fields. Theory tells us that, for decomposing non-normal incidence elastodynamic fields into upgoing and downgoing compressional waves (P-waves) and shear waves (S-waves), it is required to record, at a certain desired decomposition receiver level, all three components of the particle velocity fields and all three components of the traction tensor (Wapenaar *et al.* 1990). Depending on the setting and respective boundary conditions, certain components might vanish. For example, considering a typical land acquisition geometry with receivers placed at the Earth's surface, it is well known that the traction tensor is zero due to the Dirichlet boundary condition. As a result, MC decomposition can be carried out with three-component geophones only (e.g., Dankbaar 1985; Nakata, Snieder, and Behm 2014). At the seafloor (for example in marine ocean-bottom-cable or ocean-bottom-node acquisition), only the shear tractions vanish, such that four-component sensors are required (e.g., Schalkwijk *et al.* 2003; Amundsen and Reitan 1995). When considering an acquisitional setting with receivers placed in a horizontal or vertical borehole in the subsurface, all traction and particle velocity components are non-zero. For this case, to carry out successful elastodynamic MC field decomposition, registration of all six components is required. However, shear tractions are in general not recorded, leading to an underdetermined problem (Van der Neut, El Allouche, and Wapenaar 2010).

In recent years, we can notice an emerging acquisition design in industry that makes use of horizontal downhole sensor arrays (e.g., Bakulin *et al.* 2012a, b; Berron *et al.* 2012; Cotton and Forgues 2012). Inspired by marine acquisition designs that utilize recordings at multiple depth levels for successful field decomposition (e.g., Moldoveanu *et al.* 2007; Van Borselen, Fokkema, and Van den Berg 2013), we develop a multi-depth-level (MDL) field decomposition scheme for land acquisition. This MDL approach uses configurations with field quantity information on multiple depth levels, e.g., two horizontal boreholes that are closely separated from each other. Alternatively, a combination of a single receiver array just below a free surface combined with the natural (Dirichlet) free-surface boundary conditions could be considered as well.

The MDL decomposition scheme might provide solutions to practical issues of the MC decomposition scheme since the MDL decomposition scheme requires only specific field quantities to be recorded, and fields with different receiver signatures or noise levels can be treated separately. In modern seismic acquisition, it can be highly relevant to have a configuration of two horizontal boreholes that are closely separated from each other. Effectively, a similar acquisition geometry, with recordings at multiple depth levels, can be obtained by having a high density of vertical boreholes in a certain area (e.g., Bakulin *et al.* 2012a, b). In the fields of microseismic monitoring and passive interferometry, downhole sensors are often being deployed to reduce the noise level (e.g., Maxwell *et al.* 2010; Almagro Vidal *et al.* 2011; Xu *et al.* 2012). Applying the MDL decomposition scheme

using a single horizontal sensor array in combination with the free-surface Dirichlet boundary condition might be useful for these scenarios.

Since the principle of decomposition is not limited to acoustic fields only, we will present a unified MDL decomposition scheme that can be applied to all kinds of fields. In the appendices, we explicitly show how to apply the MDL theory to acoustic, elastodynamic, poroelastic, electromagnetic, and seismoelectric phenomena. Special attention is paid to possible issues concerning the measurability of certain fields in 2D borehole configurations.

We will illustrate the MDL decomposition first with two synthetic examples for a flux-normalized elastodynamic case. However, the MDL decomposition problem cannot always be solved. Depending on the acquisition design and the wave velocities, the problem can be ill-posed at certain (notch) frequencies. In practice, these problems can be circumvented by designing appropriate notch filters (see, e.g., Appendix A for the acoustic case). An alternative route is to integrate MC and MDL decomposition, leading to a joint inverse problem that can be solved in the least-squares sense, thereby combining the best of both worlds. We refer to this approach as MC-MDL decomposition. We demonstrate with a field data example that MC-MDL decomposition can lead to better decomposition results than pure MC decomposition since additional data are utilized.

UNIFIED THEORY OF MULTI-DEPTH-LEVEL FIELD DECOMPOSITION

Our starting point is the following matrix–vector representation of the two-way wave equation in the space–frequency domain (denoted by the hat), for a right-handed Cartesian coordinate system where the positive x_3-direction is pointing downwards (depth), i.e.,

$$\frac{\partial \hat{\mathbf{q}}(\mathbf{x},\omega)}{\partial x_3} = \hat{\mathbf{A}}(\mathbf{x},\omega)\hat{\mathbf{q}}(\mathbf{x},\omega). \tag{1}$$

Equation (1) expresses the vertical variations of the field quantities in $\hat{\mathbf{q}}(\mathbf{x},\omega)$, in terms of the medium parameters and the horizontal partial differentiation operators in matrix $\hat{\mathbf{A}}(\mathbf{x},\omega)$ acting on these field quantities (e.g., Woodhouse 1974; Kennett 1983; Ursin 1983; Wapenaar and Grimbergen 1996). The field quantities in $\hat{\mathbf{q}}$ are continuous across horizontal interfaces. Considering the fact that in the Earth the major variations occur in the depth direction, it makes sense to take the vertical axis as the direction of preference and separate the vertical variations of the field from the horizontal variations of the same field. However, the coordinate system can also be rotated, and alternative expressions can be derived in for example curvilinear coordinates (Frijlink and Wapenaar 2010). In equation (1), $\mathbf{x}$ is the space-coordinate vector (x_1, x_2, x_3), and ω represents radial frequency (we will omit these terms now for notational convenience). Throughout this paper, boldface symbols indicate vector or tensor quantities. We use $\hat{f}(x_i,\omega) = \int_{-\infty}^{\infty} f(x_i,t)e^{-j\omega t}dt$ as the definition for the forward temporal Fourier transform. Throughout this paper we consider positive ω only.

The general two-way wave equation holds for different kinds of fields in dissipative, inhomogeneous, anisotropic media, e.g., acoustic fields, electromagnetic wave and/or diffusive fields, elastodynamic fields, poroelastic fields, and seismoelectric fields (Wapenaar, Slob, and Snieder 2008). We can carry out the MDL decomposition in the space–frequency domain, making use of pseudo-differential operators as illustrated for an acoustic case in (Grimbergen, Dessing, and Wapenaar 1998). However, already for the elastodynamic system, this process is both mathematically and numerically quite tedious. In this paper, we will assume that the medium is laterally invariant at the depth level of decomposition. This assumption allows us to carry out the decomposition in the horizontal wavenumber–frequency domain (denoted by the tilde sign). We use the following definition for the forward spatial Fourier transform: $\tilde{f}(k_1,k_2,x_3,\omega) = \int_{-\infty}^{\infty}\int_{-\infty}^{\infty} \hat{f}(x_i,t)e^{jk_1x_1}e^{jk_2x_2}dx_1dx_2$. The following general relation then holds between the recorded two-way fields and the decomposed one-way fields,

$$\begin{pmatrix}\tilde{\mathbf{q}}_1\\ \tilde{\mathbf{q}}_2\end{pmatrix} = \begin{pmatrix}\tilde{\mathbf{L}}_1^+ & \tilde{\mathbf{L}}_1^-\\ \tilde{\mathbf{L}}_2^+ & \tilde{\mathbf{L}}_2^-\end{pmatrix}\begin{pmatrix}\tilde{\mathbf{p}}^+\\ \tilde{\mathbf{p}}^-\end{pmatrix}, \tag{2}$$

where the + sign indicates downgoing fields (in the positive x_3-direction) and the − sign indicates upgoing fields. For wavefields, $\tilde{\mathbf{p}}^+$ represents the one-way, decomposed downgoing field and $\tilde{\mathbf{p}}^-$ the one-way, decomposed upgoing field at a certain level of decomposition. For diffusive fields, $\tilde{\mathbf{p}}^+$ is the field that decays in the positive x_3-direction and $\tilde{\mathbf{p}}^-$ is the field that decays in the negative x_3-direction. Furthermore, $\tilde{\mathbf{L}}_1^{\pm}$ and $\tilde{\mathbf{L}}_2^{\pm}$ represent submatrices of the composition matrix $\tilde{\mathbf{L}}$ that depend on the horizontal wavenumber and the medium properties at the receiver level (e.g., Ursin 1983; Wapenaar *et al.* 2008). Decomposed fields are not uniquely defined. The fields can be normalized with respect to different quantities. Depending on our wishes, we can retrieve the upgoing and downgoing constituents of a particular field component (e.g., pressure or particle velocity normalization). Most

of the marine wavefield separation/deghosting schemes make use of either pressure or vertical component particle velocity normalization (e.g., Beasley *et al.* 2013a; Day *et al.* 2013). However, in principle, any normalization of the composition matrix will work. Throughout this paper, we will consider a normalization based on power, referred to as power-flux-normalized composition matrices. One of the advantages of using power-flux-normalization is that favourable reciprocity relations hold for the flux-normalized one-way fields (Frasier 1970; Wapenaar 1998). In equation (2), $\tilde{\mathbf{q}}_1$ represents a subvector of the two-way field quantity vector $\tilde{\mathbf{q}}$, being composed from one-way fields by applying the $\tilde{\mathbf{L}}_1^{\pm}$ submatrices to the one-way fields $\tilde{\mathbf{p}}^{\pm}$. Similarly, $\tilde{\mathbf{q}}_2$ is the subvector being composed from one-way fields by applying the $\tilde{\mathbf{L}}_2^{\pm}$ submatrices to the one-way fields $\tilde{\mathbf{p}}^{\pm}$. Note that, for both $\tilde{\mathbf{L}}$ and $\tilde{\mathbf{q}}$, the subscripts 1 and 2 do not represent spatial directions.

In the multi-component (MC) field decomposition schemes, the downgoing and upgoing one-way fields can be obtained by left-multiplying the two-way field vector with the inverse of the composition matrix:

$$\begin{pmatrix} \tilde{\mathbf{p}}^{+} \\ \tilde{\mathbf{p}}^{-} \end{pmatrix} = \begin{pmatrix} \tilde{\mathbf{L}}_1^{+} & \tilde{\mathbf{L}}_1^{-} \\ \tilde{\mathbf{L}}_2^{+} & \tilde{\mathbf{L}}_2^{-} \end{pmatrix}^{-1} \begin{pmatrix} \tilde{\mathbf{q}}_1 \\ \tilde{\mathbf{q}}_2 \end{pmatrix}. \tag{3}$$

Here, additional regularization can be applied, or alternatively, equation (3) can be solved for by a sparsity promoting algorithm (Van der Neut and Herrmann 2012). When dealing with a power-flux-normalized composition matrix, we can express the inverse of the composition matrix in terms of the transposes of the composition submatrices as follows:

$$\tilde{\mathbf{L}}^{-1}(\mathbf{k}_H) = \begin{pmatrix} -\tilde{\mathbf{L}}_2^{-}(-\mathbf{k}_H)^t & \tilde{\mathbf{L}}_1^{-}(-\mathbf{k}_H)^t \\ \tilde{\mathbf{L}}_2^{+}(-\mathbf{k}_H)^t & -\tilde{\mathbf{L}}_1^{+}(-\mathbf{k}_H)^t \end{pmatrix}. \tag{4}$$

Here, $\mathbf{k}_H = (k_1, k_2)$ is the horizontal wavenumber vector. For notational convenience, the x_3 and ω arguments are omitted here. Equation (4) generally holds, i.e., for both anisotropic and isotropic media. In case of an isotropic medium, we can organize the field quantities in $\tilde{\mathbf{q}}$ in such a way that we obtain an anti-blockdiagonal symmetry in the system matrix $\tilde{\mathbf{A}}$. In this case, the following properties hold for the composition submatrices $\tilde{\mathbf{L}}_1^{-} = \tilde{\mathbf{L}}_1^{+}$ and $\tilde{\mathbf{L}}_2^{-} = -\tilde{\mathbf{L}}_2^{+}$. As can be observed in equation (3), in order to be able to perform the up/down decomposition correctly, all two-way field components of $\tilde{\mathbf{q}}$ must have been recorded.

In the multi-depth-level (MDL) decomposition scheme, we express the one-way fields at one level in terms of the observed fields at multiple levels. In this way, we require only a certain selection of field quantities to be measured on multiple depth levels for carrying out successful up/down decomposition. With closely we here mean a distance over which it is reasonable to assume a homogeneous domain between the two depth levels or where smooth velocity variations can occur and the propagators need to be correctly estimated from the data. It is important that no reflectors are present between the two depth levels. Let us first illustrate the principle of MDL decomposition in terms of the governing matrix–vector equations. We start by defining equation (2) in terms of multiple depth levels. In this paper, we will develop MDL decomposition for the minimum requirement of two different depth levels, $x_{3;A}$ and $x_{3;B}$, where $x_{3;A} < x_{3;B}$. However, when information at more depth levels is available, this can help stabilizing the decomposition procedure (Van der Neut, Bakulin, and Alexandrov 2013). We start expressing the decomposed downgoing and upgoing power-flux-normalized fields at one depth level in terms of the observed fields at multiple levels. We do so by extrapolating one-way fields from one depth level to another, i.e.,

$$\tilde{\mathbf{p}}_B^{+} = \tilde{\mathbf{W}}^{+}(x_{3;B}, x_{3;A})\tilde{\mathbf{p}}_A^{+} \tag{5}$$

$$\tilde{\mathbf{p}}_B^{-} = \tilde{\mathbf{F}}^{-}(x_{3;B}, x_{3;A})\tilde{\mathbf{p}}_A^{-}. \tag{6}$$

When using these extrapolation operators, it is implicitly assumed that the medium between the two depth levels is source free and homogeneous. For all kinds of fields, the inverse extrapolation operator $\tilde{\mathbf{F}}^{-}(x_{3;B}, x_{3;A})$ in equation (6) is closely related to the forward propagator $\tilde{\mathbf{W}}^{+}(x_{3;B}, x_{3;A})$ as

$$\tilde{\mathbf{F}}^{-}(x_{3;B}, x_{3;A}) = (\tilde{\mathbf{W}}^{+}(x_{3;B}, x_{3;A}))^{-1}. \tag{7}$$

When we are dealing with purely propagating waves in a lossless medium, the following relation holds:

$$\tilde{\mathbf{F}}^{-}(x_{3;B}, x_{3;A}) = (\tilde{\mathbf{W}}^{+}(x_{3;B}, x_{3;A}))^{*}. \tag{8}$$

Here, the asterix (*) denotes complex conjugation. The forward extrapolation operator $\tilde{\mathbf{W}}^{+}(x_{3;B}, x_{3;A})$ extrapolates the downgoing (+) fields downwards, from depth level $x_{3;A}$ to depth level $x_{3;B}$. The inverse extrapolation operator $\tilde{\mathbf{F}}^{-}(x_{3;B}, x_{3;A})$ extrapolates the upgoing fields (-) downwards from depth level $x_{3;A}$ to depth level $x_{3;B}$. The downgoing and upgoing forward extrapolation operators $\tilde{\mathbf{W}}^{+}(x_{3;B}, x_{3;A})$ and $\tilde{\mathbf{W}}^{-}(x_{3;A}, x_{3;B})$ are defined as

$$\tilde{\mathbf{W}}^{+}(x_{3;B}, x_{3;A}) = \tilde{\mathbf{W}}^{-}(x_{3;A}, x_{3;B}) = \exp(-j\tilde{\mathbf{H}}|x_{3;B} - x_{3;A}|) \tag{9}$$

where $-j\tilde{\mathbf{H}}$ represents an n-by-n diagonal matrix containing the eigenvalues for each of the n-wavetypes present in the system under consideration (for example $n = 3$ for the elastodynamic case, where the P-wave and S-wave are the wavetypes under consideration). Note that equation (9) is a symbolic

notation (due to the use of a matrix in the argument of the exponent). Effectively, the exponent of each of the individual elements in diagonal matrix $\tilde{\mathbf{H}}$ is taken. Since we are dealing with laterally invariant media, $\tilde{\mathbf{H}}$ is a purely diagonal matrix with elements that correspond to the vertical wavenumbers $k_{3;w}$ and that can be defined for each wavetype w as

$$k_{3;w} = \sqrt{\frac{\omega^2}{\hat{c}_w^2} - \kappa^2}. \tag{10}$$

Here, the radial wavenumber is defined as $\kappa = \sqrt{k_1^2 + k_2^2}$, ω denotes the radial frequency, and $\hat{c}_w$ represents the complex, frequency-dependent velocity for each field type (Wapenaar and Berkhout 1989) (i.e., in its general form, it includes attenuation). Note that it is crucial to define the sign of the field extrapolation operators in such a way that evanescent and diffusive fields decay. The sign of the square root in equation (10) should be therefore chosen accordingly. Let us look for example at electromagnetic fields. Similar to (Amundsen *et al.* 2006), we can express the complex electromagnetic velocity as

$$\hat{c} = \frac{1}{\sqrt{\mu\bar{\varepsilon}}}, \tag{11}$$

where

$$\bar{\varepsilon} = \varepsilon + \frac{\sigma}{j\omega} \tag{12}$$

is the complex electric permittivity, consisting of the electric permittivity ε, the electric conductivity σ, and the magnetic permeability μ, which is often taken equal to the magnetic permeability in free space, i.e., $\mu_0 = 4\pi \cdot 10^{-7}$. Examining equations (11) and (12) more closely, we can distinguish three different scenarios depending on the medium parameters and the frequencies under consideration. When the term $\frac{\sigma}{j\omega} >> \varepsilon$, which is effectively the case for very low frequencies (and/or high conductivity values), we can neglect the first (electric permittivity) term, and the expression for the complex electric permittivity becomes purely imaginary. We refer to this case as purely diffusive fields (Fig. 1a). We can observe that the k_3-values in this case start at a -45° angle in the complex plane (opposite real and imaginary parts) for $\kappa = 0$ and that both the real and imaginary parts of k_3 decrease with increasing κ-values. Going towards higher frequencies (and/or lower conductivity values), the first term becomes more important, and we are dealing with a 'mixed' scenario; this scenario occurs for wave propagation in a medium with losses (Fig. 1b). In this case, the k_3-value for $\kappa = 0$ is almost purely real and moves with increasing values for κ via combinations of non-zero real and imaginary parts of k_3 towards an almost purely imaginary k_3-value. Finally, when we reach a frequency bandwidth that results in $\frac{\sigma}{j\omega} << \varepsilon$, we can neglect the second term, and the expression for the complex velocity becomes purely real in the limit. This scenario occurs for wave propagation in lossless media (Fig. 1c). Here, k_3 is in the limiting case purely real for $\kappa = 0$ and remains purely real with increasing values for κ until $\kappa^2 = \frac{\omega^2}{\hat{c}_w^2}$, which can be described as

$$k_{3;w} = \sqrt{\frac{\omega^2}{\hat{c}_w^2} - \kappa^2}, \text{ for } \kappa^2 \leq \frac{\omega^2}{\hat{c}_w^2}. \tag{13}$$

When κ then further increases,

$$k_{3;w} = -j\sqrt{\kappa^2 - \frac{\omega^2}{\hat{c}_w^2}}, \text{ for } \kappa^2 > \frac{\omega^2}{\hat{c}_w^2} \tag{14}$$

holds, resulting in purely imaginary k_3-values in the limiting case. So in this scenario, we can basically distinguish these two separate cases (for our definition of the Fourier transform).

What can be clearly observed in Fig. 1 is that, for the first and second cases (purely diffusive fields and wave propagation with losses), it is sufficient to constrain the sign of the square root such that the imaginary part of $k_3 < 0$. For the third case, since we have obtained equations (13) and (14) by taking $\lim_{\sigma \downarrow 0}$, k_3 actually still has a very small imaginary part for propagating waves. Hence, by constraining the sign of the imaginary part (equation (14)), the sign of the real part (equation (13)) is still automatically determined as well.

If σ is exactly equal to zero (and ω exactly real valued), an ambiguous situation is created for the third case of wave propagation in lossless media. To overcome this ambiguity, we then need to constrain the signs of both the real and imaginary parts of k_3. Note that in this case, equation (13) results in a purely real-valued k_3, and that equation (14) yields a purely imaginary k_3. Since we want the real part of the arguments of the exponents in equation (9) to be negative (in order to avoid that the exponents blow up), we take the negative sign of the square root in equation (14). We choose the correct sign for the real part (equation (13)) based on the fact that we desire that the phase decreases with increasing distance, whereas the amplitude stays constant. One can physically link these choices to the fact that, for propagating waves in lossless media, the amplitude remains constant (no losses), whereas the phase is decreasing with increasing distance. On the contrary, for evanescent fields in lossless media, the phase remains constant, whereas the amplitude is decreasing with increasing distance. Please note that the first case of purely diffusive fields, as described above, is in principle also a limiting case, where the $\lim_{\varepsilon \downarrow 0}$ is taken, resulting in an almost

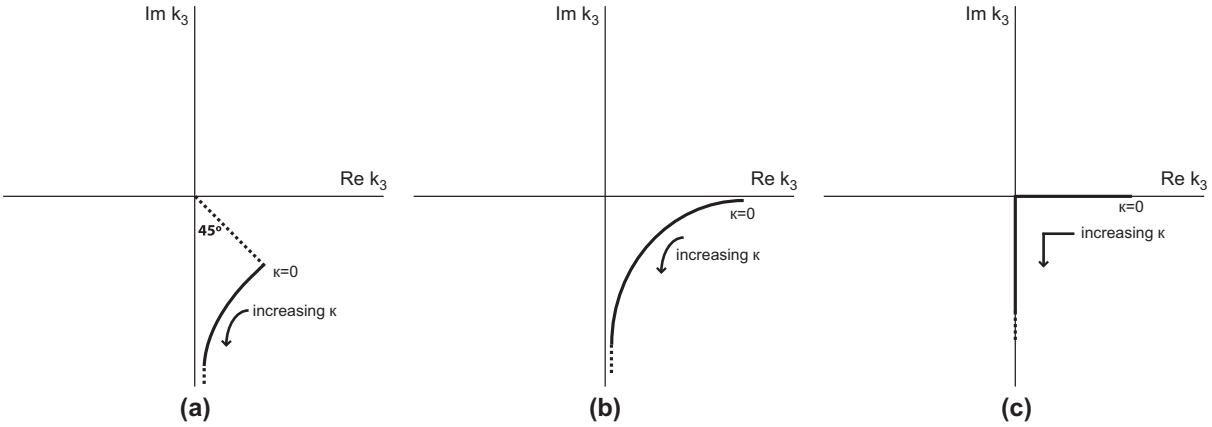

Figure 1 Real and imaginary parts of k_3 in the complex plane. (**a**) Purely diffusive fields. Only the sign of the imaginary part of k_3 needs to be constrained. (**b**) Wave propagation with losses. Only the sign of the imaginary part of k_3 needs to be constrained. (**c**) Wave propagation without losses. In this case the sign of both the real and imaginary parts of k_3 need to be constrained.

purely imaginary complex velocity. However, for this case, regardless of whether we consider the limiting case or whether we take ε exactly equal to zero, constraining the sign of the imaginary part is always sufficient to constrain the problem, as can be observed in Fig. 1(a).

Imagine now a field situation where we have obtained only $\tilde{\mathbf{q}}_2$ field quantity recordings, at different depth levels. According to equation (2) we can express the two-way field quantities of $\tilde{\mathbf{q}}_2$ recorded at depth level $x_{3;A}$ in terms of the one-way upgoing and downgoing fields as

$$\left(\tilde{\mathbf{L}}_2^+ \; \tilde{\mathbf{L}}_2^-\right)\begin{pmatrix}\tilde{\mathbf{p}}_A^+\\ \tilde{\mathbf{p}}_A^-\end{pmatrix} = \tilde{\mathbf{q}}_{2;A} \tag{15}$$

and for the recordings at depth level $x_{3;B}$

$$\left(\tilde{\mathbf{L}}_2^+ \; \tilde{\mathbf{L}}_2^-\right)\begin{pmatrix}\tilde{\mathbf{p}}_B^+\\ \tilde{\mathbf{p}}_B^-\end{pmatrix} = \tilde{\mathbf{q}}_{2;B}. \tag{16}$$

Note that the subscripts A and B have been omitted in the composition submatrices since we have already assumed that the medium is homogeneous between those two depth levels. If recordings at more than two depth levels are available, this procedure can be extended for all possible depth levels. By using equations (5) and (6), we can express the one-way fields for depth level $x_{3;B}$ also in terms of the one-way fields for level $x_{3;A}$, i.e.,

$$\left(\tilde{\mathbf{L}}_2^+\tilde{\mathbf{W}}^+ \; \tilde{\mathbf{L}}_2^-\tilde{\mathbf{F}}^-\right)\begin{pmatrix}\tilde{\mathbf{p}}_A^+\\ \tilde{\mathbf{p}}_A^-\end{pmatrix} = \tilde{\mathbf{q}}_{2;B}. \tag{17}$$

Combining equations (15) and (17) in terms of the one-way fields at depth level $x_{3;A}$, we obtain

$$\begin{pmatrix}\tilde{\mathbf{L}}_2^+ & \tilde{\mathbf{L}}_2^-\\ \tilde{\mathbf{L}}_2^+\tilde{\mathbf{W}}^+ & \tilde{\mathbf{L}}_2^-\tilde{\mathbf{F}}^-\end{pmatrix}\begin{pmatrix}\tilde{\mathbf{p}}_A^+\\ \tilde{\mathbf{p}}_A^-\end{pmatrix} = \begin{pmatrix}\tilde{\mathbf{q}}_{2;A}\\ \tilde{\mathbf{q}}_{2;B}\end{pmatrix}, \tag{18}$$

or more general

$$\tilde{\mathbf{S}}\begin{pmatrix}\tilde{\mathbf{p}}_A^+\\ \tilde{\mathbf{p}}_A^-\end{pmatrix} = \begin{pmatrix}\tilde{\mathbf{q}}_{2;A}\\ \tilde{\mathbf{q}}_{2;B}\end{pmatrix}. \tag{19}$$

Here, $\tilde{\mathbf{S}}$ represents the MDL composition matrix. When we assume that the medium properties between the levels are known (e.g., from borehole data), the extrapolators can be computed. Alternatively, one might be interested to estimate the extrapolation operators directly from the data. One way of doing this is via direct-field interferometry. For a discussion on interferometric propagator estimation, the reader is referred to Van der Neut *et al.* 2013. We have now obtained an expression relating the one-way fields at depth level $x_{3;A}$ via the MDL composition matrix $\tilde{\mathbf{S}}$ to the recorded two-way field quantities of the subvector $\tilde{\mathbf{q}}_2$ at both depth levels $x_{3;A}$ and $x_{3;B}$. By multiplying both the left-hand and right-hand sides of equation (19) with the inverse of the MDL composition matrix $\tilde{\mathbf{S}}^{-1}$, the one-way upgoing and downgoing flux-normalized fields (for each wavetype (e.g., P-waves and S-waves in the elastodynamic case)) at depth level $x_{3;A}$ can be obtained, i.e.,

$$\begin{aligned}\begin{pmatrix}\tilde{\mathbf{p}}_A^+\\ \tilde{\mathbf{p}}_A^-\end{pmatrix} &= \begin{pmatrix}\tilde{\mathbf{L}}_2^+ & \tilde{\mathbf{L}}_2^-\\ \tilde{\mathbf{L}}_2^+\tilde{\mathbf{W}}^+ & \tilde{\mathbf{L}}_2^-\tilde{\mathbf{F}}^-\end{pmatrix}^{-1}\begin{pmatrix}\tilde{\mathbf{q}}_{2;A}\\ \tilde{\mathbf{q}}_{2;B}\end{pmatrix}\\ &= \tilde{\mathbf{S}}^{-1}\begin{pmatrix}\tilde{\mathbf{q}}_{2;A}\\ \tilde{\mathbf{q}}_{2;B}\end{pmatrix}.\end{aligned} \tag{20}$$

In other words, the two-way field system under consideration has now been decomposed (for depth level $x_{3;A}$), using

only $\tilde{\mathbf{q}}_2$ field recordings at two depth levels. We can invert the modified composition matrix $\tilde{\mathbf{S}}$ numerically at each frequency and horizontal wavenumber individually. Additional regularization can be applied to solve the inverse problem. Note that, in this decomposition procedure, we treat the different vertical arrays simultaneously. The benefit of this procedure is that, instead of decomposing only for the plane-wave normal-incidence (wavenumber $k_1 = 0$) events, we decompose for all the angles of incidence. A drawback of this procedure is that since we treat everything in the horizontal wavenumber–frequency domain, our horizontal spatial sampling must fulfill the Nyquist sampling criterion. Be aware that the inversion of the composition matrix in equation (20) might not always be stable, due to the occurrence of notches at certain frequencies. The matrix inversion is unstable, when the determinant of the composition matrix is equal to zero. In other words, for certain frequency–wavenumber combinations and certain velocities and depths, the field extrapolation operators can obtain a value that makes the rows of matrix $\tilde{\mathbf{S}}$ no longer linearly independent (Van der Neut *et al.* 2013). Looking at the definitions of the field extrapolation operators (equations (9) and (10)), it can be seen that the notch frequencies are highly dependent on the vertical distance between the receiver arrays (Day *et al.* 2013). The notch problem is further addressed in Appendix A, using the acoustic representation of the field data example of this paper. Bear in mind that similar notch problems can occur for all wave and diffusion phenomena captured in this unified MDL scheme.

In addition to the notch problems, alternative instabilities can occur for example at the critical angles in the wavenumber–frequency spectrum. This is because, at the critical angle, $k_3 = 0$, and elements of the composition matrix $\tilde{\mathbf{L}}$ can contain divisions by k_3. The MDL decomposition of equation (20) will be illustrated with Synthetic Elastodynamic Example 1.

Depending on the data acquisition geometry under consideration, one might prefer to express the one-way fields at depth level $x_{3;A}$ in terms of the one-way fields at depth level $x_{3;B}$. This can be beneficial for example in passive geometries with the (earthquake or microseismic) sources below the lowest receiver level $x_{3;B}$. Slightly different to the basic case described above in equations (5) and (6), we then express the upgoing and downgoing fields at $x_{3;A}$ in terms of the upgoing and downgoing fields at $x_{3;B}$ as

$$\tilde{\mathbf{p}}_A^+ = \tilde{\mathbf{F}}^+(x_{3;A}, x_{3;B})\tilde{\mathbf{p}}_B^+ \tag{21}$$

$$\tilde{\mathbf{p}}_A^- = \tilde{\mathbf{W}}^-(x_{3;A}, x_{3;B})\tilde{\mathbf{p}}_B^-, \tag{22}$$

where

$$\tilde{\mathbf{F}}^+(x_{3;A}, x_{3;B}) = (\tilde{\mathbf{W}}^-(x_{3;A}, x_{3;B}))^{-1}. \tag{23}$$

Again, in the case of purely propagating waves,

$$\tilde{\mathbf{F}}^+(x_{3;A}, x_{3;B}) = (\tilde{\mathbf{W}}^-(x_{3;A}, x_{3;B}))^* \tag{24}$$

holds. The MDL decomposition procedure can be further modified according to one's preferences. For example, combinations of the field subvectors $\tilde{\mathbf{q}}_1$ and $\tilde{\mathbf{q}}_2$ and the corresponding submatrices of the composition matrix $\tilde{\mathbf{L}}$ might be useful. For example, when a certain depth level, in our case $x_{3;A}$ since $x_{3;A} < x_{3;B}$, coincides with the free surface of the Earth (or for example the ocean-bottom), the boundary conditions at that level might imply that certain field quantities in either $\tilde{\mathbf{q}}_1$ or $\tilde{\mathbf{q}}_2$ are equal to zero.

Let us consider this specific case, where we move depth level $x_{3;A}$ upwards such that it coincides with the Earth's free surface and where we assume that the (passive) source is located in the subsurface. We now assume that the field quantity subvector $\tilde{\mathbf{q}}_1$ is zero at the free surface due to the Dirichlet boundary condition. Hence, we do not explicitly need physical receivers at depth level $x_{3;A}$. We combine this constraint with the physical recordings of field quantity subvector $\tilde{\mathbf{q}}_2$ at depth level $x_{3;B}$.

Analogous to equation (20), we can then obtain the one-way upgoing and downgoing fields at depth level $x_{3;B}$, by solving

$$\begin{aligned}\begin{pmatrix}\tilde{\mathbf{p}}_B^+\\ \tilde{\mathbf{p}}_B^-\end{pmatrix} &= \begin{pmatrix}\tilde{\mathbf{L}}_1^+\tilde{\mathbf{F}}^+ & \tilde{\mathbf{L}}_1^-\tilde{\mathbf{W}}^-\\ \tilde{\mathbf{L}}_2^+ & \tilde{\mathbf{L}}_2^-\end{pmatrix}^{-1}\begin{pmatrix}\tilde{\mathbf{q}}_{1;A}=0\\ \tilde{\mathbf{q}}_{2;B}\end{pmatrix}\\ &= \tilde{\mathbf{S}}^{-1}\begin{pmatrix}\tilde{\mathbf{q}}_{1;A}=0\\ \tilde{\mathbf{q}}_{2;B}\end{pmatrix}.\end{aligned} \tag{25}$$

Alternatively, one could derive explicit expressions for $\tilde{\mathbf{p}}_B^+$ and $\tilde{\mathbf{p}}_B^-$ using analytical expressions for the inverse of the composition matrix, yielding

$$\tilde{\mathbf{p}}_B^+ = \left[\tilde{\mathbf{L}}_2^+ - \tilde{\mathbf{L}}_2^-\{\tilde{\mathbf{L}}_1^-\tilde{\mathbf{W}}^-\}^{-1}\tilde{\mathbf{L}}_1^+\tilde{\mathbf{F}}^+\right]^{-1}\tilde{\mathbf{q}}_{2;B} \tag{26}$$

$$\tilde{\mathbf{p}}_B^- = \left[\tilde{\mathbf{L}}_2^- - \tilde{\mathbf{L}}_2^+\{\tilde{\mathbf{L}}_1^+\tilde{\mathbf{F}}^+\}^{-1}\tilde{\mathbf{L}}_1^-\tilde{\mathbf{W}}^-\right]^{-1}\tilde{\mathbf{q}}_{2;B}. \tag{27}$$

The system of the wave/field phenomenon under consideration has now been decomposed (for depth level $x_{3;B}$), using only the field quantity recordings of field subvector $\tilde{\mathbf{q}}_2$ measured at depth level $x_{3;B}$, combined with the fact that the field quantities of the subvector $\tilde{\mathbf{q}}_1$ at level $x_{3;A}$ are zero. Note that if $x_{3;A}$=$x_{3;B}$, equation (25) reduces to the MC decomposition scheme of equation (3). The application of equation

(25) will be illustrated with Synthetic Elastodynamic Example 2. Interesting to mention is the similarity between equation (25) and deghosting procedures (e.g., Fokkema and Van den Berg 1993; Frijlink *et al.* 2011). However, in equation (25), the deghosting procedure is expressed more generally, holding for all kinds of fields.

We can summarize the MDL decomposition theory using a general notation, distinguishing between decomposition at the upper depth level and decomposition at the lower depth level (hereby still assuming that $x_{3;A} < x_{3;B}$). For the decomposition at the upper level, we would like to express the one-way fields at level $x_{3;B}$ in terms of the one-way fields at $x_{3,A}$, i.e,

$$\begin{pmatrix} \tilde{\mathbf{L}}_j^+ & \tilde{\mathbf{L}}_j^- \\ \tilde{\mathbf{L}}_k^+\tilde{\mathbf{W}}^+ & \tilde{\mathbf{L}}_k^-\tilde{\mathbf{F}}^- \end{pmatrix} \begin{pmatrix} \tilde{\mathbf{p}}_A^+ \\ \tilde{\mathbf{p}}_A^- \end{pmatrix} = \begin{pmatrix} \tilde{\mathbf{q}}_{j;A} \\ \tilde{\mathbf{q}}_{k;B} \end{pmatrix}, \tag{28}$$

where j and k can take up the values 1 or 2, and j is not necessarily equal to k. Similarly, for the decomposition at the lower level, we express the one-way fields at level $x_{3;A}$ in terms of the one-way fields at $x_{3,B}$, i.e,

$$\begin{pmatrix} \tilde{\mathbf{L}}_j^+\tilde{\mathbf{F}}^+ & \tilde{\mathbf{L}}_j^-\tilde{\mathbf{W}}^- \\ \tilde{\mathbf{L}}_k^+ & \tilde{\mathbf{L}}_k^- \end{pmatrix} \begin{pmatrix} \tilde{\mathbf{p}}_B^+ \\ \tilde{\mathbf{p}}_B^- \end{pmatrix} = \begin{pmatrix} \tilde{\mathbf{q}}_{j;A} \\ \tilde{\mathbf{q}}_{k;B} \end{pmatrix}. \tag{29}$$

Equations (28) and (29) form the basis of the MDL field decomposition scheme. Theoretically, one can even set up the decomposition problem in a similar way as equations (28) and (29) but then trying to obtain one-way fields at both depth levels, e.g., $\tilde{\mathbf{p}}_B^+$ and $\tilde{\mathbf{p}}_A^-$.

When looking at equations (28) and (29), we can observe that, in order to successfully carry out MDL up/down field decomposition, we either need field quantity recordings at at least two depth levels $x_{3;A}$ and $x_{3;B}$, or recordings at one depth level $x_{3;B}$ combined with boundary conditions at depth level $x_{3;A}$. One can imagine that, instead of measuring the full field quantity subvectors $\tilde{\mathbf{q}}_1$ or $\tilde{\mathbf{q}}_2$ and their corresponding submatrices $\tilde{\mathbf{L}}_{1,2}$, one wishes to select only a few, easily measurable or well-constrained field quantities of $\tilde{\mathbf{q}}_1$ and $\tilde{\mathbf{q}}_2$ to solve the decomposition problem. By selecting the desired rows of the composition submatrices corresponding with the selected field quantities, the MDL decomposition can be carried out. Be aware that this can only be done if the selected rows that compose the matrix $\tilde{\mathbf{S}}$ have sufficient rank. In other words, the matrix to be inverted should not be rank-deficient. If the matrix is full rank, the custom character of the adapted composition matrix $\tilde{\mathbf{S}}$ will not cause any additional problems since the decomposition matrix is obtained via numerical inversion. The customly defined combinations of measured or boundary condition-defined field quantities and selected composition submatrix rows are not explicitly defined in the general scheme of equations (28) and (29). Here, we only want to point out the possibility of these kinds of combinations.

Please remain aware that the equations above are defined in the horizontal wavenumber–frequency domain, implicitly assuming lateral invariance at the depth level of decomposition. A similar scheme can be developed in the space–frequency domain for inhomogeneous media, using pseudo-differential operators (e.g., Fishman, McCoy, and Wales 1987; Grimbergen *et al.* 1998; Wapenaar, Dillen, and Fokkema 2001; Wapenaar *et al.* 2008). However, already for the elastodynamic case, the space-frequency derivations become quite a tedious exercise, both analytically and numerically.

Now that we have obtained a unified MDL decomposition scheme, we can apply the scheme to different wave phenomena. The Appendices A–E show in more detail how to apply the scheme when dealing with acoustic, elastodynamic, poroelastic, electromagnetic, and seismoelectric fields. Throughout this paper, we will consider geometries where horizontal boreholes are located in the subsurface. The MDL decomposition scheme is then applied to obtain up/down field separation. In addition to up/down decomposition, the scheme also decomposes the field quantities into its different wave modes. One can theoretically imagine that, when considering surface measurements at several horizontal spatial locations and rotating the geometry of the MDL scheme, one might also apply the MDL decomposition principles to field left/right decomposition.

We will start illustrating the principle of the MDL decomposition scheme further with two synthetic flux-normalized elastodynamic examples. In this case, $\tilde{\mathbf{q}}_1 = -\tilde{\boldsymbol{\tau}}_3$, and $\tilde{\mathbf{q}}_2 = \tilde{\mathbf{v}}$, and the flux-normalized composition matrix $\tilde{\mathbf{L}}$ is chosen according to Wapenaar *et al.* (2008). Here, $\tilde{\boldsymbol{\tau}}_3$ represents the traction vector acting at a horizontal plane, and $\tilde{\mathbf{v}}$ denotes the particle velocity vector. Note that, for these two synthetic examples, no approximations regarding amplitudes have been made. After the synthetic elastodynamic examples, we will present an acoustic representation of a field land data example where the MC and MDL decomposition schemes are combined.

Before we look in closer detail to the examples, let us make some final but crucial remarks regarding borehole measurements. First of all, one can imagine that, if the receivers are placed in a horizontal borehole, this results in a 'line' measurement. Let us for example consider a horizontal borehole in the x_1-direction. Then, when we consider propagation/diffusion in a 3D medium, out-of-plane waves/fields are still taken into account; hence, variations of a certain field quantity in the

x_2-direction are still considered (e.g., Bleistein, Cohen, and Hagin 1987; Bleistein 1987). This is called the 2.5D situation. In contrast, we can consider a purely 2D situation where effective line sources in, for example, the x_2-direction are considered. In this situation, the field quantity components have no variations with respect to the x_2-direction. The resulting data are referred to as 2D (e.g., Bleistein *et al.* 1987; Bleistein 1987). In the 2D scenario, natural mode separation can occur for elastodynamic (P-SV and SH mode), electromagnetic (TE and TM mode), or seismoelectric (SH-TE and P-SV-TM mode) phenomena.

In addition, the type of borehole also plays a crucial role. For example, if the borehole has a concrete casing and is filled with a fluid, this has consequences for the receivers and types of fields that can be recorded. For example, theoretically, no shear waves will be measurable inside the borehole if it is fluid-filled. Certain field quantities might then be zero at for example depth level $x_{3;B}$, whereas the field quantity is theoretically non-zero and measurable (in absence of the borehole). However, in practice, shear waves are routinely measured in for example vertical seismic profiling and logging using sensors in a fluid-filled borehole (e.g., Cheng and Toksöz 1981). In this paper, we will develop everything from an ideal theoretical point of view. Keep in mind that, in reality the situation is far more complex. Fluid-filled boreholes modify the responses as, for example, formulated by Peng, Cheng, and Toksöz (2003). This does not necessarily mean that the MDL decomposition scheme does not work. On the contrary, having for example shear wave measurements available in fluid-filled boreholes might help the MDL decomposition scheme (it does need additional calibration).

In case of electromagnetic fields, metallic borehole casings can cause problems as well. In the following synthetic examples, we assume that the receivers are buried on a horizontal line in the subsurface but not placed in a fluid-filled borehole. In the field data example presented afterwards, the receivers are similarly placed in the subsurface. We will use an acoustic scheme for decomposing this data set.

Synthetic elastodynamic example 1: configuration with two receiver depth levels

To illustrate the MDL decomposition approach, we will apply the method to a synthetic elastodynamic example, using equation (20). We make use of a 2D elastodynamic finite-difference model (Thorbecke and Draganov 2011), where receivers are being placed at two depth levels $x_{3;A} = 1000$ m and $x_{3;B} = 1010$ m, below a strongly reflecting salt body (see Fig. 2). We consider the plane spanned by x_1 and x_3. Hence, the fields in the x_2-direction in the field vector of Appendix C decouple. The P-wave and S-wave velocities for the layer in which the receivers are located are 2500 m/s and 1800 m/s, respectively. The density of the layer is 1500 kg/m^3. The source is a monopole pressure source with a peak frequency of 20 Hz. We use the more stable, alternative 2D versions of the power-flux-normalized composition matrix $\tilde{\mathbf{L}}$, as presented by Wapenaar *et al.* (2008). Figure 3 represents the original shot records as recorded at depth level $x_{3;A}$, with the two-way physical field quantities τ_{13}, τ_{33}, v_1, and v_3. Due to the complexity of the model, upgoing and downgoing events are interfering. Furthermore, the presence of the strongly reflecting salt body results in strong differences in amplitudes between downgoing and upgoing events.

We now carry out both MC and MDL field decomposition, resulting in the decomposed fields of Fig. 4, where the MC decomposed one-way fields are shown in black and the MDL decomposed fields in red (dashed). There is an excellent match in both amplitude and phase. In other words, the MDL decomposition scheme manages to retrieve the correct one-way fields at $x_{3;A}$ using only particle velocities at $x_{3;A}$ and $x_{3;B}$. There is a difference for the first upgoing P-wave event (Fig. 4c). The MC decomposition scheme shows a (black) event where this event is absent for the MDL decomposition scheme. Evaluation turns out that this is leakage from the strong downgoing P-wave energy. This is most likely caused by small numerical errors in the computed pressure fields (in combination with the large relative strength of this downgoing event), which had to be interpolated in time and space to align with the particle velocity fields, because a staggered grid has been used in the finite difference code (Virieux 1986). The MDL decomposition scheme does not suffer from this problem since it only uses particle velocity data.

For the MDL decomposition, we have carried out a damped least squares inversion of the customized composition matrix $\tilde{\mathbf{S}}$, using a Tikhonov regularization with a damping factor of $1e^{-4}$ of the maximum amplitude of $\tilde{\mathbf{S}}\tilde{\mathbf{S}}^{\dagger}$. Here the dagger sign denotes the complex conjugate transpose.

It is very nice to see the effect of the strongly reflecting salt body. One can observe in the downgoing fields (for both P- and S-waves) three pronounced downgoing events, corresponding to the direct downgoing field and the internal multiples within the salt layer. Also when looking at the two-way input data, one can clearly see that the upgoing fields are obscured due to the presence of the salt body. However, after decomposition, the upgoing fields are clearly distinguishable and similar results are obtained for the MC decomposition

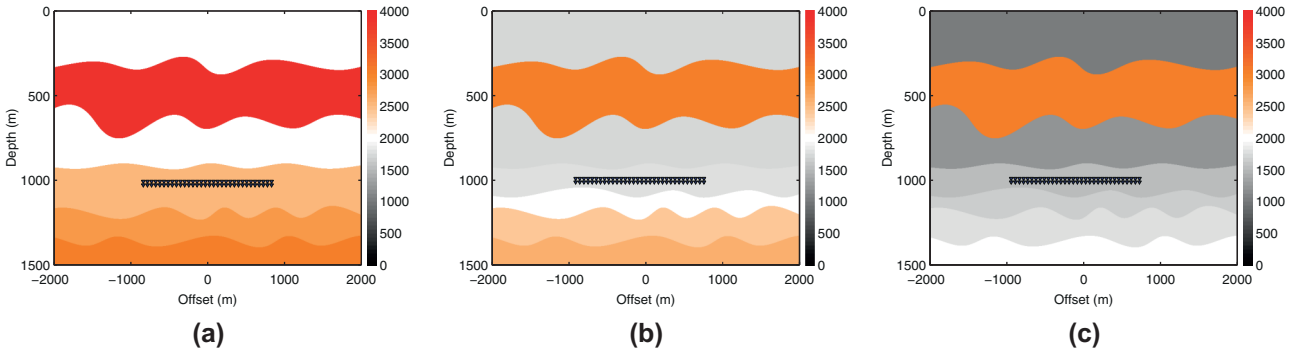

Figure 2 Geometry of synthetic elastodynamic example 1. (**a**) The colors represent P-wave velocities in m/s. (**b**) The colors represent S-wave velocities in m/s. (**c**) The colors represent density values in kg/m^3.

and the MDL decomposition methods. In addition, the MC and MDL decomposition schemes are handling the interference between upgoing and downgoing fields equally well.

Note that for a 2.5D scenario, $\tilde{\tau}_{23}$ and $\tilde{v}_2$ should be measured for MC decomposition, and only $\tilde{v}_2$ should be measured additionally for MDL decomposition. Similar results are then to be expected.

Synthetic elastodynamic example 2: Configuration with a single horizontal sensor array below a free surface

As mentioned above, the MDL decomposition procedure is fully customizable according to one's preferences. Here we will consider a special case, moving depth level $x_{3;A}$ upwards such that it coincides with the Earth's free surface. Effectively, we have an acquisition geometry consisting of a single horizontal sensor array combined with a free-surface constraint. We will use equation (25) as the governing equation of the MDL decomposition scheme matching the acquisition geometry under consideration. Again, a 2D finite-difference elastodynamic model will be used, with receivers placed only at $x_{3;B}$, at 5 m depth. We first consider a homogeneous medium. The P-wave velocity of the medium is 2000 m/s, the S-wave velocity 1400 m/s, and the density is 1000 kg/m^3. A 45° (anti-clockwise) oriented dipole force source with a peak frequency of 20 Hz, buried at 2000 m depth, is considered the (passive) source. The only upgoing fields to be expected are one upgoing P-wave and one upgoing SV-wave. At the free surface, P-SV field conversion can occur (Aki and Richards 1980). Therefore, we expect two downgoing P-wave events (P-P and SV-P) and two downgoing SV-wave events (P-SV and SV-SV).

The originally recorded two-way fields are presented in Fig. 5. Due to the 45° anti-clockwise diagonally oriented force source, the recorded fields reveal asymmetric amplitudes along the hyperbolas. We again compare the results of the MC decomposition and the MDL decomposition approach in Fig. 6. The black lines represent the one-way fields at depth level $x_{3;B}$ obtained via MC decomposition. In this case, both stress and particle velocity measurements were required. The MDL decomposition results are displayed in red (dashed). These up/down and wave mode decomposed fields were obtained using only particle velocity recordings at $x_{3;B}$ combined with the free-surface Dirichlet boundary condition of zero traction. One can clearly observe that the MDL approach, using now only particle velocity data at one depth level, again retrieves the correct one-way fields. There is a perfect match in both phase and amplitude. In addition, the decomposition results show indeed only the expected one-way fields, i.e., one upgoing P-wave events, and two downgoing SV-wave, two downgoing P-wave events, and two downgoing SV-wave events. Again, by measuring additionally $\tilde{\tau}_{23}$ and $\tilde{v}_2$ for MC decomposition and only $\tilde{v}_2$ as extra quantity for MDL decomposition, similar results are to be expected for the 2.5D scenario.

The downgoing field can be interpreted as the elastodynamic free-surface ghost of the upgoing field. The proposed algorithm can therefore be used for elastodynamic deghosting. This can be very useful for passive data processing, for instance for passive seismic interferometry (Draganov, Wapenaar, and Thorbecke 2006; Xu *et al.* 2012). In addition, decomposition has been used in combination with multi-dimensional deconvolution of passive recordings at the surface (Nakata *et al.* 2014). Using MDL decomposition, similar multi-dimensional deconvolution procedures can be carried out on passive data with receivers located in the subsurface (which might lead to a better signal-to-noise ratio of the recordings) (Almagro Vidal *et al.* 2014; Almagro Vidal and Wapenaar 2014).

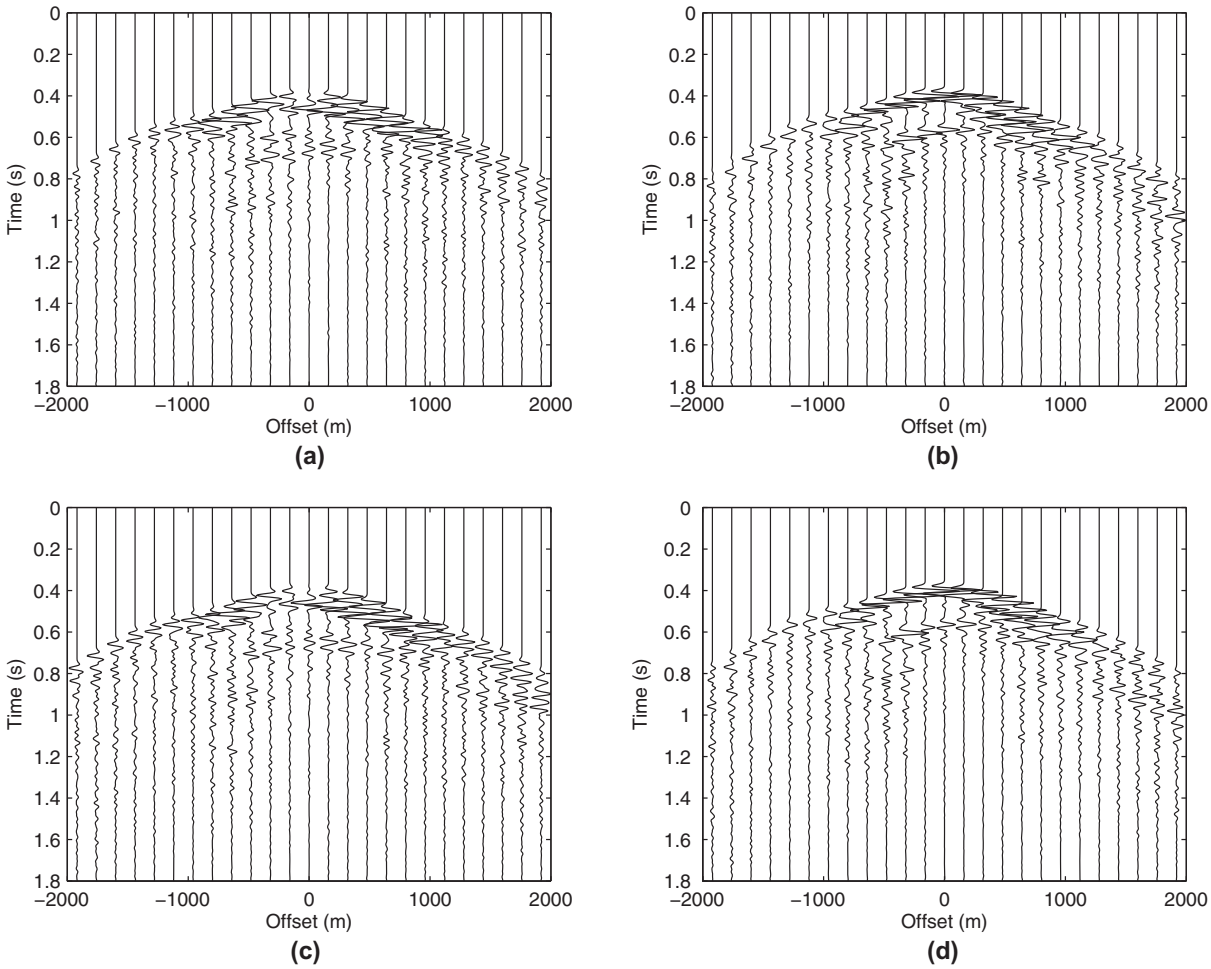

Figure 3 Original shot records registered at depth level $x_{3;A} = 1000$ m. (**a**) Two-way data $-\tau_{13}$. (**b**) Two-way data $-\tau_{33}$. (**c**) Two-way data v_1. (**d**) Two-way data v_3.

So far, we have only considered scenarios where the correct velocity has been used at the decomposition level as well as for extrapolating the fields between the different depth levels. We will now investigate the sensitivity of the MDL decomposition scheme to errors in the velocity model. We therefore consider the same acquisition geometry as described for the homogeneous example above but now with a velocity model that experiences a horizontal gradient from −20% velocity error to +20% velocity error with respect to the homogeneous P- and S-wave velocities (see Fig. 7). The resulting two-way data are presented in Fig. 8. We apply MC and MDL decomposition using the homogeneous velocities. In this way, the effects of using erroneous velocities on both the MC and MDL decomposition scheme are investigated.

The results of both decomposition schemes are displayed in Fig. 9. In black, the results of MC decomposition using an erroneous velocity at the depth level of decomposition are displayed. In red dash, the results of applying MDL decomposition with erroneous velocities at the depth level of decomposition and for the extrapolation operators are displayed. We can observe that the downgoing P-field and S-field are correctly resolved and equally-well in terms of both phase and amplitude. The upgoing P-field and S-field show leakage of downgoing energy (indicated by the arrows) but again, the amount of leakage is comparable for the MC and MDL decomposition schemes. However, please note that it is crucial to have properly dealt with the notch problems (due to, for example, notch filters) or that the distance over which extrapolation takes place is small enough to avoid notches that overlap with the data bandwidth. If this is namely not the case, the undesired notch effects on the decomposition results will become more pronounced when using incorrect velocity models.

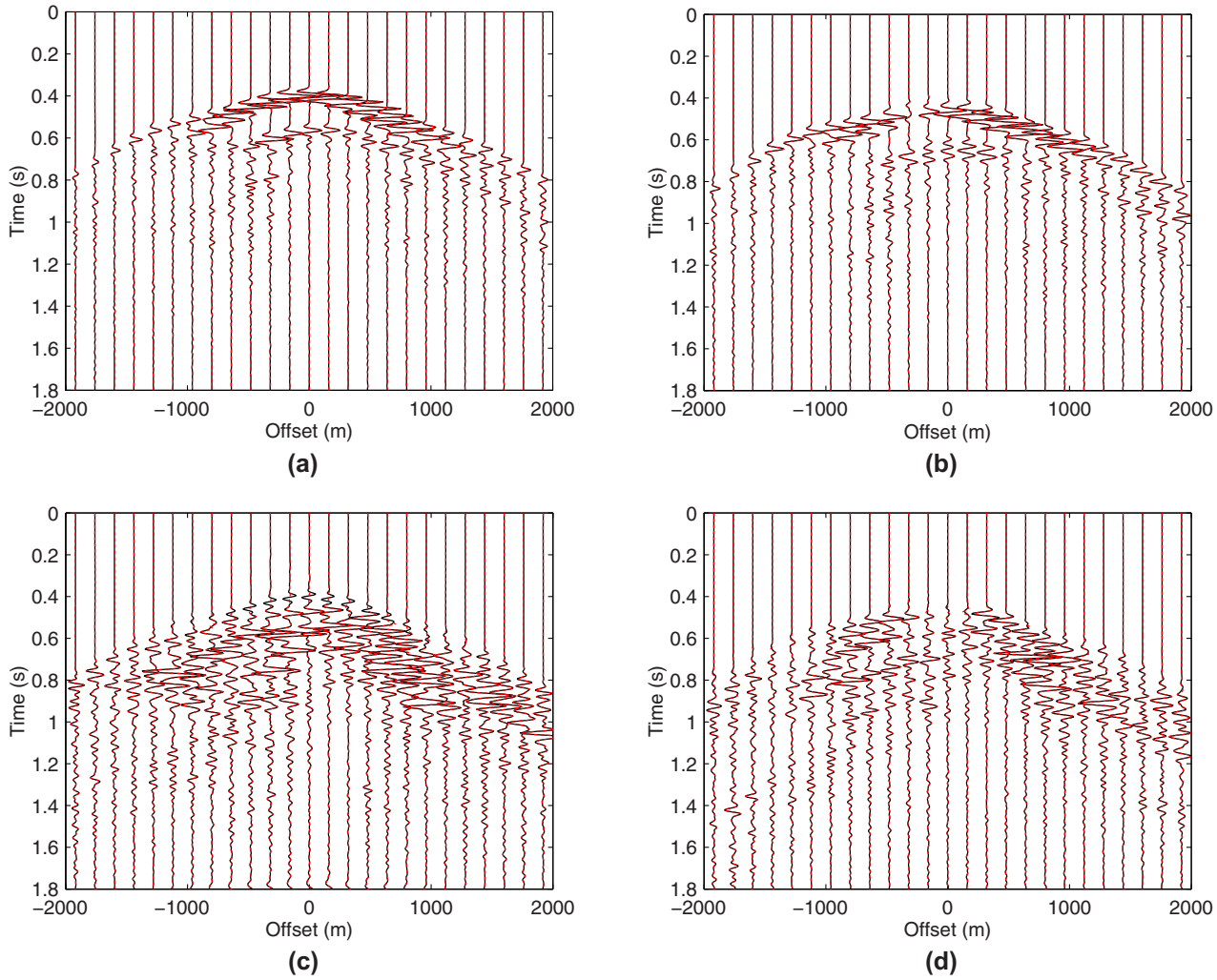

Figure 4 Comparison between the MC decomposition results in black and the MDL decomposition results in red (dashed). (**a**) Downgoing P-waves. (**b**) Downgoing S-waves. (**c**) Upgoing P-waves. (**d**) Upgoing S-waves.

Since we are here effectively considering a laterally varying medium, which is a realistic scenario for (near-surface) land data, we know that, theoretically, the applied horizontal wavenumber–frequency decomposition approach is not valid. We predict that the leakage (for both decomposition schemes) can be avoided when carrying out the field decomposition in the space–frequency domain (e.g., Grimbergen *et al.* 1998).

For the MDL decomposition, we have carried out a damped least-squares inversion of the customized composition matrix $\tilde{\mathbf{S}}$, using a Tikhonov regularization with a damping factor of $1e^{-4}$ of the maximum amplitude of $\tilde{\mathbf{S}}\tilde{\mathbf{S}}^{\dagger}$.

MC-MDL acoustic decomposition applied to a field land data set

Theory of the MC-MDL decomposition

Following the MC decomposition procedure, upgoing and downgoing one-way fields can be obtained by inverting the forward problem of equation (2). In the MDL decomposition scheme, the decomposition problem is treated slightly different. We have seen that, using field extrapolation operators, we can express the one-way fields at one depth level in terms of the observed fields at multiple levels. The synthetic elastodynamic examples have shown that the MDL up/down

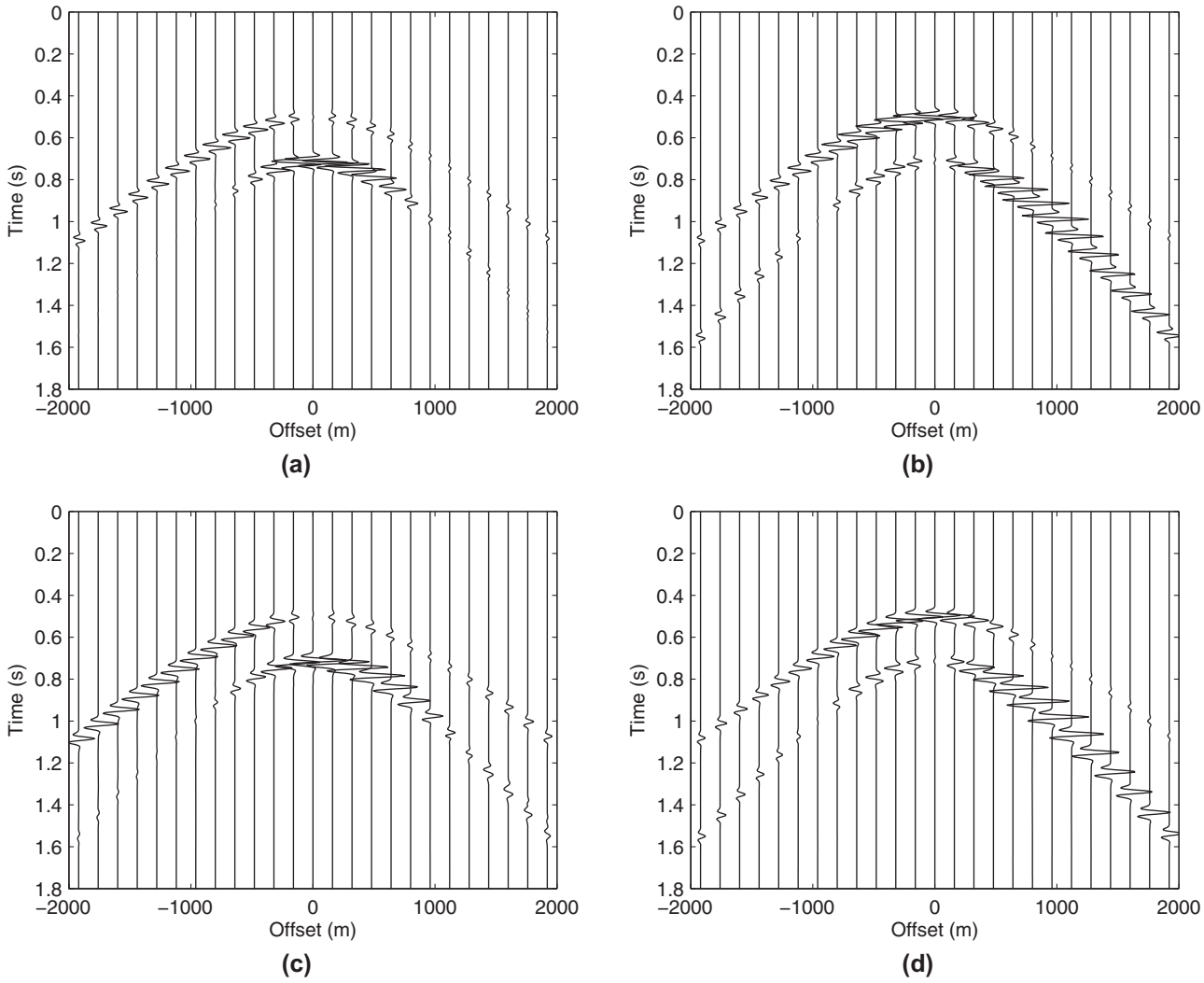

Figure 5 Original shot records for a homogeneous model registered at depth level $x_{3;B} = 5$ *m*. (**a**) Two-way data $-\tau_{13}$. (**b**) Two-way data $-\tau_{33}$. (**c**) Two-way data v_1. (**d**) Two-way data v_3.

decomposition obtains correct one-way fields in both amplitude and phase. However, as discussed in Appendix A for acoustic fields, the MDL inversion can suffer from notches at certain frequencies. The MC decomposition scheme does not suffer from these notches but might suffer from different sensor characteristics (Schalkwijk *et al.* 2003) or the fact that differently recorded field quantities might not be of similar quality due to different noise levels (Burnstad *et al.* 2012). The success of the MDL decomposition scheme on synthetic data combined with the discussion of the notch problems has led to the idea of combining the MC decomposition scheme with the MDL decomposition schemes (MC-MDL), thereby combining the best of both worlds. We will investigate this idea by applying it to an acoustic representation of a real land data set recorded in Annerveen, the Netherlands. Here, the aim is to perform up/down field separation at depth level $x_{3;B}$.

We start by looking at the decomposition problem as an inverse problem. Using equation (2) as the basic equation, we try to improve the decomposition with an additional inversion constraint: the free-surface condition from the MDL decomposition scheme, where depth level $x_{3;A}$ coincides with the free surface. This corresponds to the Annerveen acquisition geometry, where $x_{3;A} = 0$ m, and $x_{3;B} = 50$ m. This leads to the following overdetermined inverse problem:

$$\begin{pmatrix} \tilde{\mathbf{q}}_{1;B} \\ \tilde{\mathbf{q}}_{2;B} \\ \mathbf{0} \end{pmatrix} = \begin{pmatrix} \tilde{\mathbf{L}}^{+}_{1;B} & \tilde{\mathbf{L}}^{-}_{1;B} \\ \tilde{\mathbf{L}}^{+}_{2;B} & \tilde{\mathbf{L}}^{-}_{2;B} \\ \tilde{\mathbf{L}}^{+}_{1;A}\tilde{\mathbf{F}}^{+} & \tilde{\mathbf{L}}^{-}_{1;A}\tilde{\mathbf{W}}^{-} \end{pmatrix} \begin{pmatrix} \tilde{\mathbf{p}}^{+}_{B} \\ \tilde{\mathbf{p}}^{-}_{B} \end{pmatrix}. \tag{30}$$

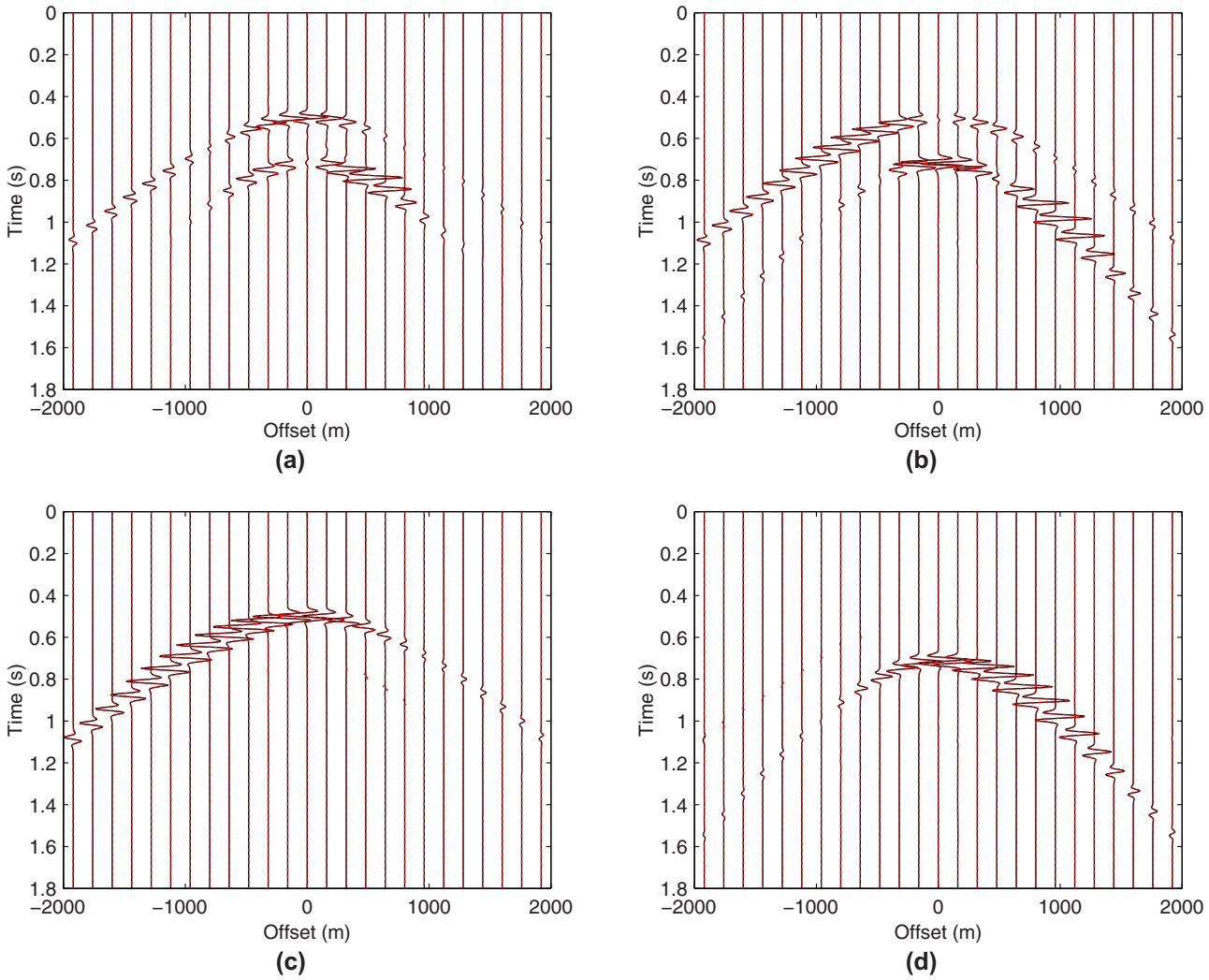

Figure 6 Comparison between the MC decomposition results in black and the MDL decomposition results in red (dashed) for the homogeneous model. (**a**) Downgoing P-waves. (**b**) Downgoing S-waves. (**c**) Upgoing P-waves. (**d**) Upgoing S-waves.

For our field data example, we will consider scalar versions of equation (2), referred to as the MC decomposition problem, and equation (30), referred to as the MC-MDL decomposition problem. Here, $\tilde{q}_1 = \tilde{p}$, i.e., acoustic pressure field, and $\tilde{q}_2 = \tilde{v}_3$, i.e., vertical component of the particle velocity (see also Appendix A for an extensive discussion on acoustic MDL field decomposition). The flux-normalized scalars $\tilde{L}_1^{\pm}$ and $\tilde{L}_2^{\pm}$, as well as the scalar field extrapolation operators $\tilde{W}^{-}$ and $\tilde{F}^{+}$, are taken as defined by Wapenaar (1998). For clarity, the subscripts A and B have been added in equation (30). However, as discussed earlier, we assume that the medium between depth levels $x_{3;A}$ and $x_{3;B}$ is homogeneous. Although the distance between $x_{3;A}$ and $x_{3;B}$ is only 50 m and taking into account the near-surface geology of this specific part of the Netherlands, this seems a valid assumption. Due to this assumption, we can omit the subscripts of the composition submatrices. As can be observed, the added row in equation (30) overdetermines the inverse problem but does not require additionally recorded fields. The added equation makes use of the Dirichlet free-surface boundary condition, i.e., the pressure at the free surface equals zero. We will now investigate whether this overdetermined inverse problem improves the decomposition results of the Annerveen data set. The inverse problem will be solved in the least squares sense. Again, other approaches, such as sparsity promotion (Van der Neut and Herrmann 2012), could also be considered. For both the MC and MC-MDL decomposition, we have carried out a damped least squares inversion of the (customized) composition matrix $\tilde{\mathbf{S}}$, using a Tikhonov regularization with a damping factor of $1e^{-4}$ of the maximum amplitude of $\tilde{\mathbf{S}}\tilde{\mathbf{S}}^{\dagger}$.

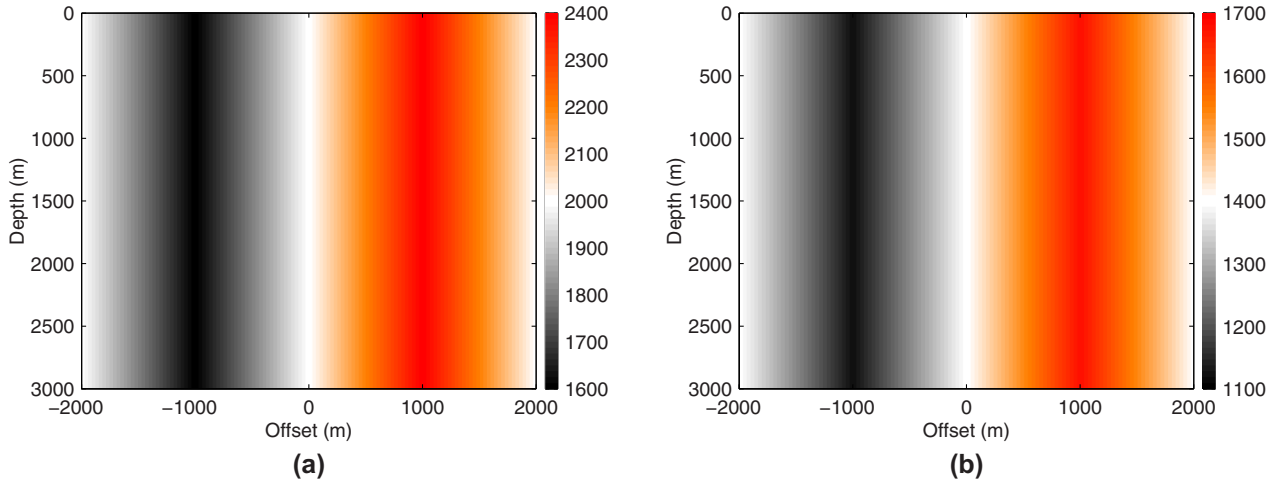

Figure 7 Geometry of synthetic elastodynamic example 2 with velocity variations of -20% to +20% with respect to the homogeneous velocities. (**a**) The colors represent P-wave velocities in m/s. (**b**) The colors represent S-wave velocities in m/s.

Up/down decomposition results of the Annerveen data set. The data have been acquired on land in Annerveen, located in the North of the Netherlands. One receiver array consisting of 96 receivers with a spacing of 11.75 m was buried at 50 m depth. In addition, 144 shots were fired at 4 m depth with a source spacing of 11.75 m, alternating positions with respect to the receiver positions. The receivers have registered both the pressure and vertical-component particle velocity fields.

Several initial data processing steps need to be performed before we carry out the field decomposition. We use standard filtering techniques to filter out the surface waves. In addition, all dead traces are removed. Since we are dealing with a pseudo-2D data set, we correct the amplitudes by multiplying with the square root of time. In addition, the data show quite a variety in amplitudes for different shots. Therefore, we carry out a shot normalization, where we normalize the shot gathers with the power of each shot. Since the MC-MDL decomposition scheme assumes depth level $x_{3;A}$ to be coinciding with the free surface of the Earth and depth level $x_{3;B}$ corresponding to the receiver level at 50 m depth, one can directly notice that our source in this configuration is located between the two depth levels. The theory does not account for this configuration. This has to do with the fact that, in the derivation of the field extrapolation operators (Wapenaar 1998), it is assumed that no sources are located between the depth levels. However, by removing the incident fields from the data set (i.e., direct field and direct source ghost), the MC-MDL decomposition can still be applied to the remaining reflected data set. We remove these direct fields by applying a time gate, which has been selected by visual inspection (Fig. 10).

We carry out the visual inspection looking at an average over ten adjacent common-source gathers. The underlying assumption of this approach is that the Earth is laterally invariant over the distance of these ten shots, which is a reasonable assumption considering the area of interest.

The crucial parameter for our acoustic MC-MDL decomposition that needs to be determined is the P-wave velocity in the layer between depth levels $x_{3;A}$ and $x_{3;B}$. The P-wave velocity determines, via the vertical wavenumber k_3, the forward and inverse extrapolation operators $\tilde{W}^{-}$ and $\tilde{F}^{+}$, respectively. Furthermore, the P-wave velocity is an important constituent in the composition matrix $\tilde{\mathbf{L}}$ (Wapenaar 1998). Here, we determine the P-wave velocity by looking at the arrival time difference between a strong upgoing reflection, and its receiver side ghost. To identify these two events, we make use of the two individual pressure and particle velocity data sets, and exploit our knowledge about polarity reversal of registered events. Effectively, this means that p and v_3 have opposite polarity for the first upgoing reflection but identical polarities for the later arriving receiver side ghost. This can be clearly observed in Fig. 10, indicated by the two arrows. Based on the zero-offset time difference between those two events and knowing the propagation pathlength ($2 \times 50 = 100$ m), the P-wave velocity can be estimated. Our best estimate of the P-wave velocity is $c_P = 1639$ m/s. Exact knowledge of the density is not required since it appears as a scalar that occurs in each element of the composition matrix. To precondition the inversion, we scale composition matrix element $\tilde{L}_2$ from Wapenaar (1998) with the impedance (with the density taken as 1 kg/m^3), resulting in a better-posed inverse problem.

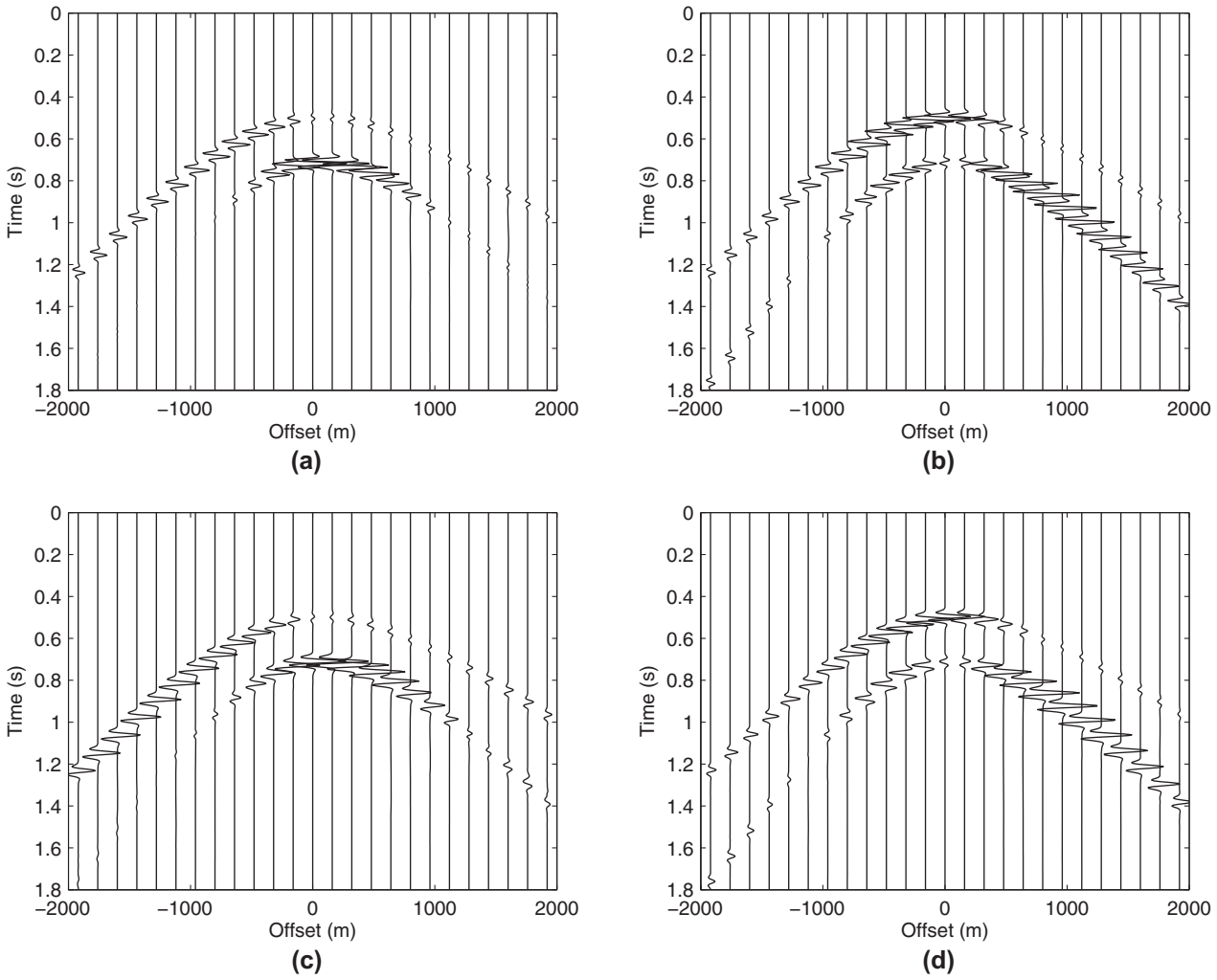

Figure 8 Original shot records registered at depth level $x_{3;B} = 5\ m$, for the velocity model with velocity variations of -20% to +20% with respect to the homogeneous velocities. (**a**) Two-way data $-\tau_{13}$. (**b**) Two-way data $-\tau_{33}$. (**c**) Two-way data v_1. (**d**) Two-way data v_3.

We start with the MC field decomposition, according to equation (2). Since both the pressure and particle velocity data are involved simultaneously in the MC decomposition schemes, we want to make sure that the sensors are correctly calibrated. Therefore, we focus on a clear event in the two-way recorded data set and select a data window around this event. We select the top black box, as indicated in Fig. 11. The event in this data window is a purely upgoing event. We therefore want to minimize the downgoing energy in this data window. We use a least-squares minimization subtraction algorithm to find the correct scaling factor between the pressure and particle velocity data that minimizes the downgoing energy and to scale the data accordingly. We now carry out the MC decomposition, resulting in the decomposed flux-normalized one-way fields shown in Fig. 12(a, b).

Next, we focus on the MC-MDL decomposition. Looking at row 3 of equation (30), we observe that the following relation must hold at the free surface:

$$\tilde{L}_1^+ \tilde{F}^+ \tilde{p}_B^+ = -\tilde{L}_1^- \tilde{W}^- \tilde{p}_B^-. \tag{31}$$

This equation also holds for an individual event. We enforce equation (31) to hold by selecting a certain upgoing event and its corresponding downgoing event, indicated with the two boxes in Fig. 11. The term $\tilde{L}_1^+ \tilde{p}_B^+$ then corresponds to the selected downgoing event in the two-way pressure data set, illustrated by the dark green boxes in Fig. 11, and $\tilde{L}_1^- \tilde{p}_B^-$ to the selected upgoing event in the two-way pressure data set, indicated by the black boxes in Fig. 11. We will propagate the two-way data set, including the selected upgoing event, forward (in the propagation direction) to the free

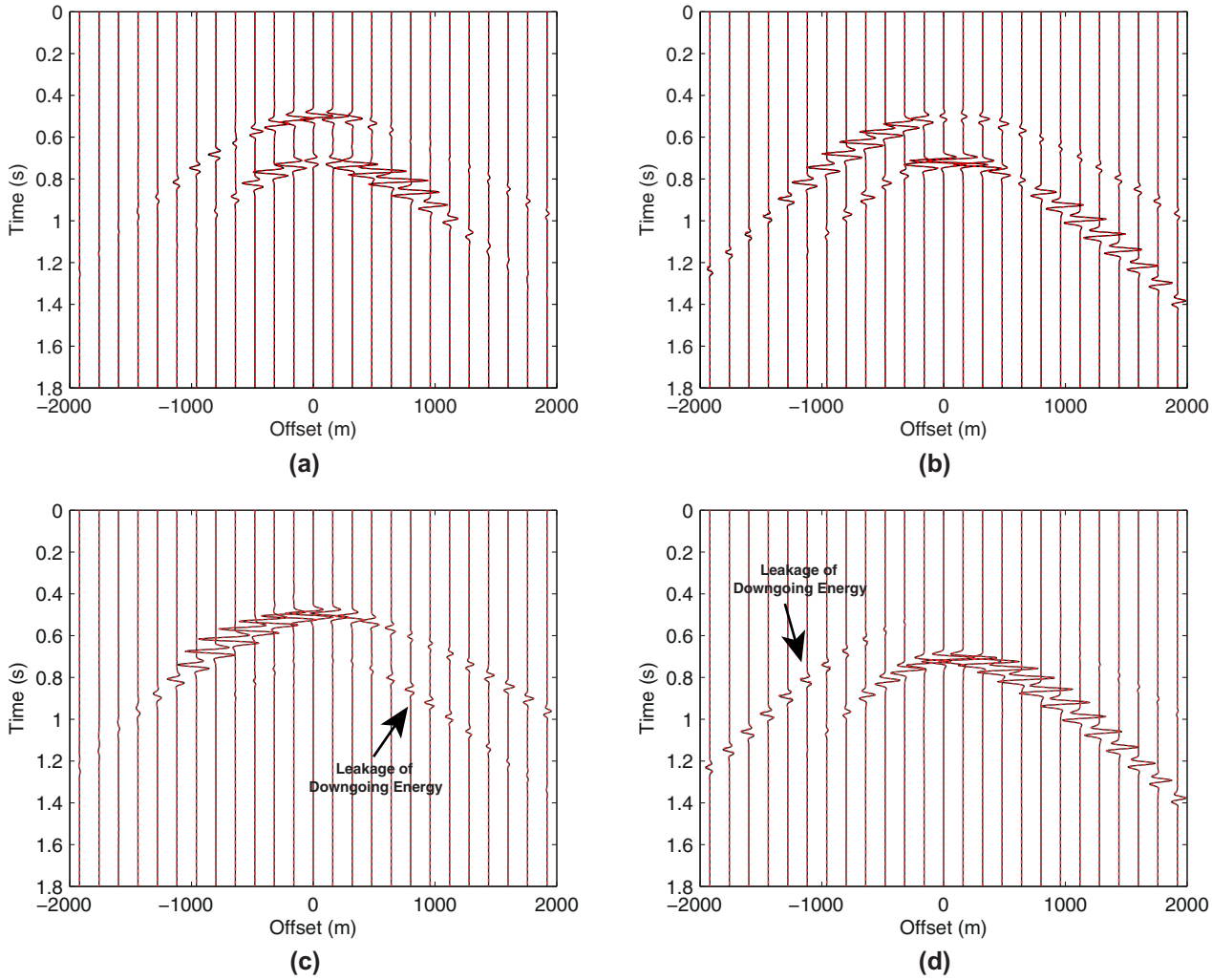

Figure 9 Comparison between the MC decomposition results in black and the MDL decomposition results in red (dashed) for the velocity model with velocity variations of -20% to +20% with respect to the homogeneous velocities. (**a**) Downgoing P-waves. (**b**) Downgoing S-waves. (**c**) Upgoing P-waves. (**d**) Upgoing S-waves.

surface using $\tilde{W}^{-}$. Secondly, we will propagate the two-way data set, including the selected downgoing event, backward (against the propagation direction) to the free surface. Here, equation (31) must hold. We now calibrate the two shifted two-way events at the free surface with each other, using a least squares minimization subtraction algorithm on the selected event. A similar minimization problem has been defined for the vertical-component particle velocity field. Both minimization problems are solved for simultaneously. We then apply this calibration factor to the composition matrix element containing $\tilde{F}^{+}$, corresponding to the downgoing fields (see equation (30)). The overall weight of the extra equation in the inversion can be further tuned according to preference.

We are now all set to carry out the MC-MDL field decomposition. The decomposition is carried out by least squares in version of equation (30).

Figures 12(a) and 12(b) display the upgoing and downgoing MC decomposed fields. The results of the overdetermined MC-MDL decomposition problem are shown in Figures 12(c) and (d). What can be clearly observed is that by adding the extra constraint to the inversion (the third row in the composition matrix of equation (30)), we have improved the decomposition results, especially for the downgoing fields (compare Fig. 12b and d). In addition, it can be observed that the MC decomposition result has vertical 'white' bands at certain offsets, corresponding to dead or noisy traces in the two-way recorded data. Our MC-MDL

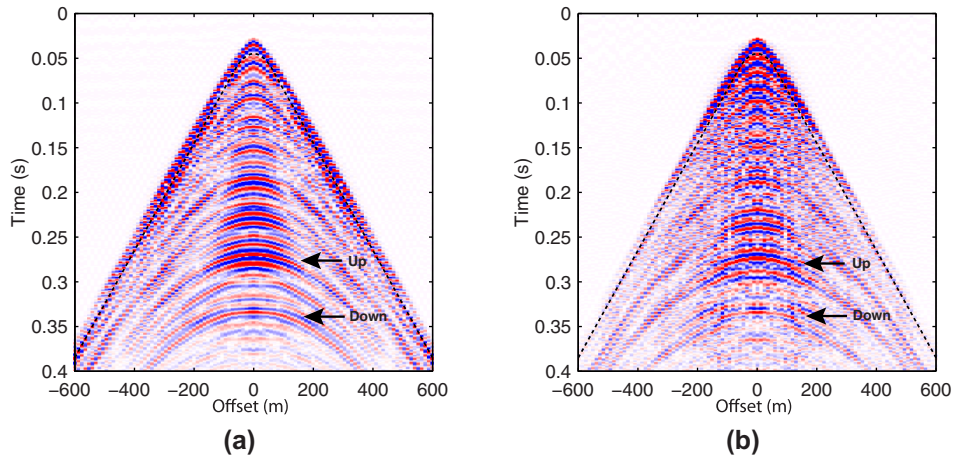

Figure 10 Average over ten common-source gathers. The black line represents the start of the Hanning taper, separating incident fields from reflected fields, and has a taper length of ten samples downwards. The black arrows indicate a strong upgoing reflection and its receiver side ghost. We make use of our knowledge of polarity reversal between the two data sets to estimate the P-wave velocity. (**a**) Pressure data p. (**b**) Vertical component particle velocity data v_3.

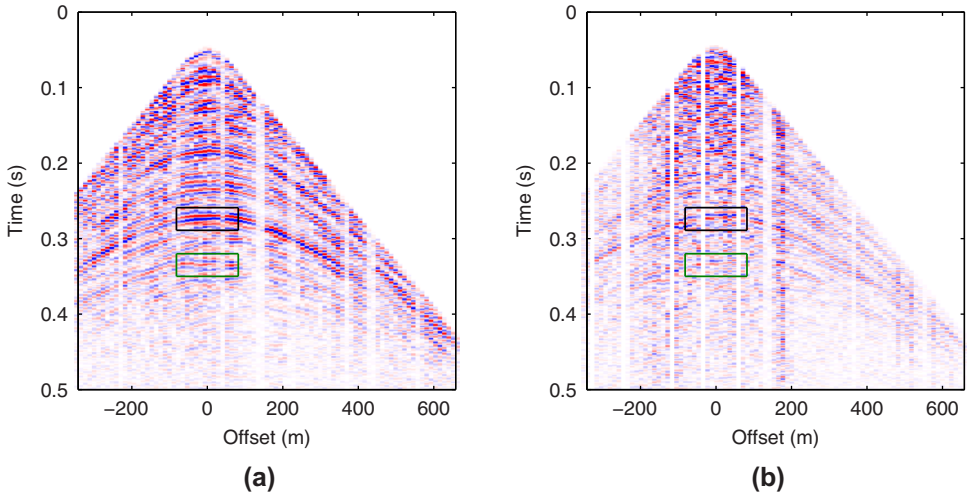

Figure 11 Two-way reflected data. The boxes represent selected windows for data calibration. The black boxes is used for calibrating $\tilde{p}$ and $\tilde{v}_3$ in MC decomposition. The black and the dark green boxs are used for up/down calibration in the MDL decomposition scheme. (**a**) Pressure data p. (**b**) Vertical component particle velocity data $v3$.

decomposition result does not show these 'white' bands so strongly. This is due the applied field extrapolation operators in the wavenumber–frequency domain, implicitly yielding an interpolation between the traces.

DISCUSSION

We have shown that the MDL decomposition scheme correctly decomposes different kinds of fields. However, the MDL scheme might suffer from invertibility issues due to the presence of notches. The notch problems have been investigated more closely for an acoustic example (Appendix A). We have shown that notch filters can be designed such that the MDL field decomposition for the acoustic case can still be carried out using only pressure or particle velocity recordings. Similar notch filters might be required for the other field phenomena treated in the appendices. The notch filters remove certain (notch) frequencies from the data. Which frequencies are missing depends on which data set is used for the decomposition. Since, for the acoustic case, the pressure and vertical-component particle velocity data are complementary to each other, combining the two data sets will result again in full-bandwidth decomposed fields.

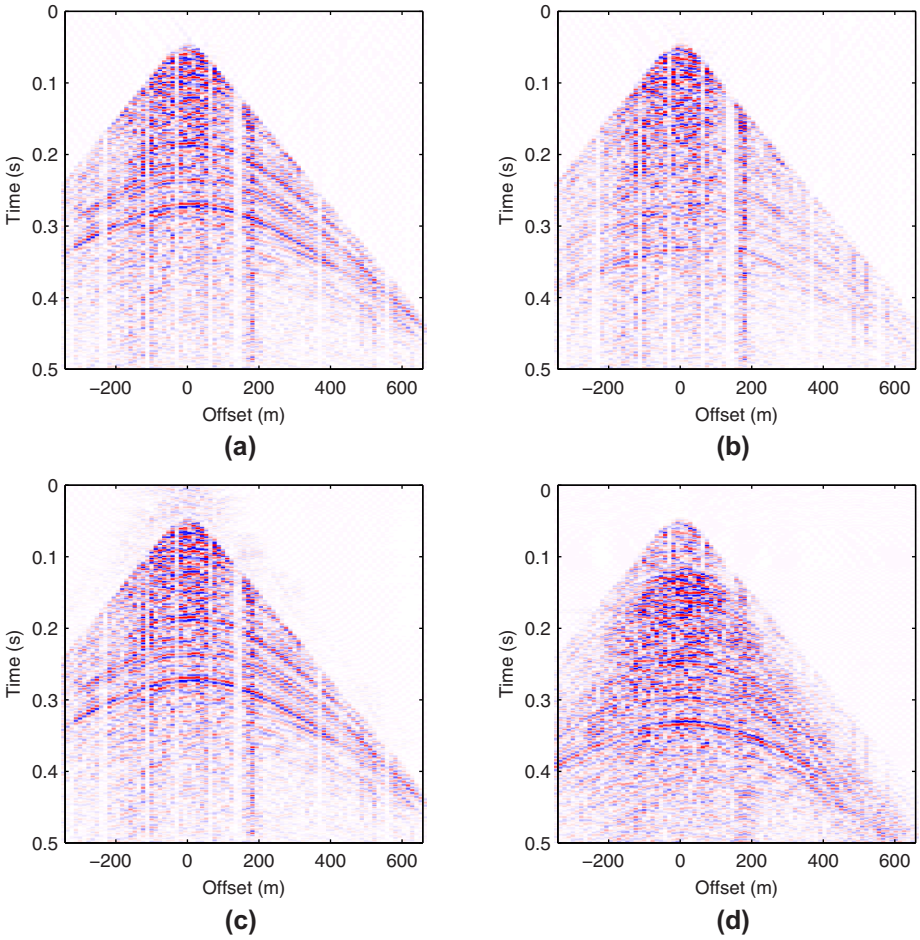

Figure 12 Comparison of the decomposition results of the Annerveen land data set. (**a**) MC decomposed upgoing fields. (**b**) MC decomposed downgoing fields. (**c**) MC-MDL decomposed upgoing fields. (**d**) MC-MDL decomposed downgoing fields.

A way to avoid suffering from notches in the frequency spectrum of the data is to carry out deghosting in the space–time domain. Using single-component measurements only (e.g., only pressure data), Beasley *et al.* (2013a, b) showed that, by using the wave equation to simulate upgoing and downgoing wavefield propagation between the receiver level and the water surface, wavefield separation can be achieved. In addition, Robertsson and Amundsen (2014) showed that, by using finite-difference modeling to predict ghosts from upgoing waves (after removal of the direct wave) and by instantaneously injecting these predicted ghosts, destructive interference takes place with the recorded ghosts. In this way, successful deghosting in the space–time domain is achieved, without suffering from notches. Furthermore, Amundsen and Robertsson (2014) have presented a similar method for deghosting in the space–time domain that relies on multi-component (MC) recordings. An important challenge of these space–time domain decomposition approaches based on wave propagation is the fact that they require unaliased data and hence fine receiver sampling (Beasley *et al.* 2013a). For 3D deghosting, this fine sampling is also required in the cross-line direction. In order for the method to work, the water velocity, receiver depth, and receiver positions must be known. However, these are mainly challenges that also hold for most other deghosting procedures (including our MDL decomposition scheme). If one would like to apply a similar space–time domain approach to land data, the fact that the velocities are required to be known might be problematic, and one should carefully investigate the sensitivity of this method to the use of incorrect velocity models. The same holds for the MDL decomposition scheme, for which we investigated the velocity sensitivity in Synthetic Elastodynamic Example 2.

As we discussed in Appendix A, we can straightforwardly add the pressure and vertical-component particle velocity data

(with some calibration factor) to obtain the full-frequency spectrum decomposed fields. Alternatively, one might for example prefer to combine the two data sets in a very late stage. One possible way would be via multi-dimensional deconvolution (Wapenaar *et al.* 2008). The multi-dimensional deconvolution method can be useful, for example, for surface- and sea bottom-related multiple elimination (Wapenaar and Verschuur 1996; Amundsen 1999). Via multi-dimensional deconvolution, which makes use of upgoing and downgoing (flux-normalized) fields, the reflection response of the medium below a certain depth level can be obtained, as if the medium above this depth level was homogeneous. The multi-dimensional deconvolution procedure can be applied to different types of fields (Amundsen and Holvik 2004; Holvik and Amundsen 2005; Van der Neut *et al.* 2010; Wapenaar *et al.* 2008). Instead of adding the pressure and vertical-component particle velocity data to obtain full-frequency spectrum decomposed fields, we can alternatively combine these two data sets smoothly at the stage of multi-dimensional deconvolution, thereby exploiting the benefit of treating the two data sets separately until a very late stage of the imaging workflow. Despite the problem of the notches, one of the benefits of applying MDL decomposition based on either pressure or vertical-component particle velocity data independently (for the acoustic case) is that sensor calibration (as is needed for MC decomposition) is not required. Combining these two data sets in the stage of multi-dimensional deconvolution also avoids the need of sensor calibration since the same sensor calibration functions act on both the upgoing and downgoing fields. Therefore, they will occur at both the left-hand and right-hand sides of the multi-dimensional deconvolution equations to be solved and will drop out of the equations automatically.

The MDL decomposition scheme makes use of recordings at multiple depth levels. So far, we have shown land data examples, where recordings in a horizontal borehole (or recordings using a high-density of vertical boreholes) on land were used. More generally speaking, the MDL scheme needs recordings at multiple depth levels, applicable to any medium. One can think of combining for example marine (dual) streamer data with ocean-bottom-node data.

CONCLUSIONS

Applying field decomposition to a real data set is often quite challenging. The multi-component (MC) field decomposition scheme makes use of differently recorded field components, e.g., both pressure (p) and vertical-component particle velocity (v_3) data in a purely acoustic case. In practice, recordings can be obscured by different sensor characteristics, requiring calibration with an unknown calibration factor. In addition, not all field quantities required for MC field decomposition might be available, and they may not always be of similar quality due to different noise levels. In particular, when dealing with more complex field phenomena (e.g., elastodynamic or seismoelectric fields), the MC field up/down decomposition requires measuring many different field quantities.

We have presented a multi-depth-level (MDL) field decomposition scheme for land acquisition that is inspired by marine acquisition designs that make use of recordings at multiple depth levels for successful field decomposition. Our MDL decomposition approach makes use of configurations with field quantity information on multiple depth levels, e.g., two horizontal boreholes that are closely separated from each other, or a combination of a single receiver array just below a free surface, thereby exploiting the natural (Dirichlet) free-surface boundary conditions.

We have theoretically described the MDL decomposition approach in a unified form, showing that, in principle, it can be applied to different kinds of fields in dissipative, inhomogeneous, anisotropic media, such as for example acoustic fields, electromagnetic fields, elastodynamic systems, poroelastic fields, and seismoelectric fields. The theoretical details of decomposing each of these types of fields, for laterally invariant media at the depth level of decomposition, are given in the Appendices A–E.

Assuming that the medium is laterally invariant at the depth level of decomposition allows us to carry out the MDL decomposition in the horizontal wavenumber–frequency domain. We have illustrated the MDL decomposition scheme using two synthetic elastodynamic modeling examples. We have first demonstrated that the MDL decomposition scheme leads to correctly retrieved power-flux-normalized one-way fields, for both P- and S-waves, using only particle velocity recordings at two depth levels. Secondly, we showed that, when we have particle velocity recordings at one depth level, in combination with the free-surface Dirichlet boundary condition of zero traction, we can correctly decompose the data into one-way fields as well. Comparison with MC obtained decomposed fields shows a perfect match in both amplitude and phase for both cases.

We have additionally tested the effects of using erroneous velocities on both the MC and MDL decomposition schemes. For the considered example, we observed that the downgoing P- and S- fields are correctly and equally well resolved in terms of both phase and amplitude. The upgoing P- and

S- fields show leakage of downgoing energy, but the amount of leakage is comparable for the MC and MDL decomposition schemes. Please note that it is crucial to have properly dealt with possible notch problems. Otherwise, the undesired notch effects on the decomposition results will become more pronounced when using incorrect velocity models.

We have shown that the MDL decomposition scheme is fully customizable to the acquisition geometry and measured field quantities under consideration. Care must be taken that the customized composition matrix to be inverted is always of sufficient rank. However, depending on the acquisition design and wave velocities under consideration, notches may occur at certain frequencies, causing the customizable MDL composition matrix to become uninvertible. Additional notch filters are then required.

The success of the MDL decomposition scheme on the synthetic elastodynamic data, combined with the problem of the notches, has led to the idea of combining the MC and MDL decomposition schemes. The decomposition problem is in principle an inverse problem. By adding an extra equation of the MDL decomposition scheme to the MC composition matrix, we can overdetermine the inverse problem and hereby better constrain the inversion. Since this equation makes use of the Dirichlet free-surface boundary condition, where for the acoustic case the pressure at the free surface equals zero, we do not require additionally recorded fields for this extra inversion constraint. Comparison of the results of this overdetermined MC-MDL decomposition scheme with the results of the conventional MC field decomposition clearly showed improvements in the obtained one-way flux-normalized fields, especially for the downgoing fields.

ACKNOWLEDGEMENTS

The authors would like to thank Jan Thorbecke for the availability of his elastodynamic finite-difference synthetic modeling code 'fdelmodc'. In addition, we thank 'LOFAR' for the availability of the Annerveen data set. We also highly appreciate the useful suggestions of reviewer Andrey Bakulin and an anonymous reviewer, as well as the (associate) editor.

APPENDIX A

ACOUSTIC FIELD DECOMPOSITION, NOTCHES AND FILTERS

In this appendix we closely investigate the notch patterns for an acoustic case and show that acoustic MDL decomposition can also be carried out using only pressure or vertical-component particle velocity data, in combination with notch filters. We use a scalar version of equation (2) as the basic starting equation for field decomposition, where we take $\tilde{q}_1 = \tilde{p}$ and $\tilde{q}_2 = \tilde{v}_3$. Here, $\tilde{p}$ corresponds to the acoustic pressure field, and $\tilde{v}_3$ denotes the vertical-component particle velocity field. We will focus on single horizontal downhole sensor arrays combined with a free-surface constraint, which corresponds to the acquisition geometry of our presented field data example. Let us consider two scalar versions of equation (29), where level $x_{3;A}$ coincides with the free surface and level $x_{3;B}$ is located at some arbitrary shallow depth level, measuring either pressure or vertical-component particle velocity fields. We locate the source for example at the free surface. This leads to

$$\begin{pmatrix} \tilde{p}_B^+ \\ \tilde{p}_B^- \end{pmatrix} = \begin{pmatrix} \tilde{L}_1^+ \tilde{F}^+ & \tilde{L}_1^- \tilde{W}^- \\ \tilde{L}_1^+ & \tilde{L}_1^- \end{pmatrix}^{-1} \begin{pmatrix} \tilde{q}_{1,A} \\ \tilde{q}_{1,B} \end{pmatrix} = \tilde{\mathbf{S}}_p^{-1} \begin{pmatrix} \tilde{q}_{1,A} \\ \tilde{q}_{1,B} \end{pmatrix}, \tag{A1}$$

where, as defined above, $\tilde{q}_1 = \tilde{p}$ and to

$$\begin{pmatrix} \tilde{p}_B^+ \\ \tilde{p}_B^- \end{pmatrix} = \begin{pmatrix} \tilde{L}_1^+ \tilde{F}^+ & \tilde{L}_1^- \tilde{W}^- \\ \tilde{L}_2^+ & \tilde{L}_2^- \end{pmatrix}^{-1} \begin{pmatrix} \tilde{q}_{1,A} \\ \tilde{q}_{2,B} \end{pmatrix} = \tilde{\mathbf{S}}_{v_3}^{-1} \begin{pmatrix} \tilde{q}_{1,A} \\ \tilde{q}_{2,B} \end{pmatrix}, \tag{A2}$$

where $\tilde{q}_2 = \tilde{v}_3$. As can be seen, the same downgoing and upgoing decomposed fields at depth level $x_{3;B}$ can be obtained in two independent ways. We can either apply the inverse of the MDL composition matrix $\tilde{\mathbf{S}}_p^{-1}$ to a zero value of the pressure field at level $x_{3;A}$ combined with a measured pressure field at $x_{3;B}$ (equation (A1)), or apply the inverse $\tilde{\mathbf{S}}_{v_3}^{-1}$ to a zero pressure field at level $x_{3;A}$ combined with a measured vertical particle velocity at level $x_{3;B}$ (equation (A2)). Here, $\tilde{L}_1^{\pm}$ and $\tilde{L}_2^{\pm}$ are again taken as defined in Wapenaar (1998). However, notches occuring at certain notch frequencies can cause the $\tilde{\mathbf{S}}$ matrix to become uninvertible. In both our elastodynamic synthetic examples, the distance was small enough to avoid suffering from notches when solving the inverse problem. However, for certain distances, notches will occur at certain frequencies overlapping with the data band. In these cases, additional notch filters are required in order to be able to invert the MDL composition matrices correctly. In our field data example, we combined MC with MDL decomposition, such that we did not suffer from the notches. Alternatively, the following approach could be taken.

From a mathematical point of view, we expect the notches to occur in those situations where the determinant of the composition matrix to be inverted $\tilde{\mathbf{S}}_{p;v_3}$ becomes zero (or close to zero). By evaluating when the determinant becomes zero (or close to zero), we can analytically obtain information about the specific notch frequency patterns at which the matrix becomes uninvertible (or poorly invertible). Starting from equation (A1), we can determine the notch patterns for the pressure data. We can see that in the case of a zero-determinant, the following equation holds:

$$\tilde{L}_1^+ \tilde{L}_1^- \left[\tilde{F}^+ - \tilde{W}^-\right] = 0. \tag{A3}$$

In addition to the the zero-solutions for $\tilde{L}_1^{\pm}$ (or for $\tilde{L}_2^{\pm}$ in case of equation (A2)), the term in between the square brackets can be zero. Considering propagating waves, we can apply equation (24) leading to

$$\tilde{L}_1^+ \tilde{L}_1^- \left[\left(\tilde{W}^-\right)^* - \tilde{W}^-\right] = 0. \tag{A4}$$

Rewriting the term in the square brackets using Euler's formula yields the following relation describing the notch patterns

$$\begin{aligned}\left(\tilde{W}^-\right)^* - \tilde{W}^- &= -2j\Im\{\tilde{W}^-\} \\ &= -2j\sin\left(-k_3|x_{3;B} - x_{3;A}|\right) = 0.\end{aligned} \tag{A5}$$

When we start from equation (A2), we can obtain the notch patterns for the vertical-component particle velocity data in a similar way. We can use the following properties $\tilde{L}_1^- = \tilde{L}_1^+$ and $\tilde{L}_2^- = -\tilde{L}_2^+$. This leads to the following zero-determinant condition:

$$\tilde{L}_1^{\pm} \tilde{L}_2^+ \left[-\tilde{F}^+ - \tilde{W}^-\right] = 0. \tag{A6}$$

Considering propagating waves, we can again apply equation (24) leading to

$$\tilde{L}_1^{\pm} \tilde{L}_2^+ [-(\tilde{W}^-)^* - \tilde{W}^-] = 0. \tag{A7}$$

Rewriting the term in the square brackets using Euler's formula yields the following relation describing the notch patterns

$$\begin{aligned}-(\tilde{W}^-)^* - \tilde{W}^- &= -2\Re\{\tilde{W}^-\} \\ &= -2\cos\left(-k_3|x_{3;B} - x_{3;A}|\right) = 0.\end{aligned} \tag{A8}$$

We can clearly observe that the notch patterns for the pressure and vertical-component particle velocity data follow a complementary trigonometric pattern (sine or cosine) with identical argument. This complementary pattern has been widely exploited for marine/ocean-bottom-cable deghosting procedures (e.g., Day *et al.* 2013).

As an alternative approach, as known from inverse theory, the condition numbers can provide us with information about the invertibility of a certain matrix. The condition number represents the ratio between the largest and smallest singular values of the matrix. High condition numbers indicate that the matrix is poorly conditioned and therefore difficult to invert (Van der Neut *et al.* 2013). Investigating the invertibility of $\tilde{\mathbf{S}}_{p,v_3}$ by looking at 1/(Condition Number) clearly shows us the locations of the notches for both the pressure and vertical-component particle velocity data (see Figures 13(a) and 13(b), respectively). Since we here display the inverse of the condition numbers, low values correspond to the notch frequencies for that specific type of data. One can see that the two types of data are indeed complementary to each other. In other words, where a notch occurs for the pressure data at a certain frequency-wavenumber combination, the particle velocity field can provide the data and *vice versa*.

We have designed two filters that follow these notch patterns and are also complementary to each other. To exploit the fact that the filters should be complementary to each other, we have used $\sin^2(a) + \cos^2(a) = 1$. In this way, we try to find a certain a that matches the notch patterns, such that a maximum contribution is given to the maximum amplitudes in the inverse condition number plots (corresponding to low condition numbers and good matrix invertibility) and a minimum contribution is given to the minimum amplitudes in the inverse condition number plots. Using the analytical solutions of equations (A5) and (A8), we have found that $a = k_3(x_{3;B} - x_{3;A})$ exactly follows the moveout patterns in the wavenumber–frequency plots. The notch filters are therefore taken as $w_p = \sin^2(k_3(x_{3;B} - x_{3;A}))$ and $w_{v_3} = 1 - w_p$, for the pressure field and vertical-component particle velocity field data, respectively (see Fig. 14).

Applying these filters to the MDL decomposition matrices $\tilde{\mathbf{S}}_{p,v_3}^{-1}$ avoids suffering from the notches in the MDL decomposition. In this way, the acoustic field up/down decomposition can be carried out using either solely pressure recordings at $x_{3;B}$ combined with a free-surface, zero-pressure constraint or solely vertical-component particle velocity recordings at $x_{3;B}$ combined with a free-surface, zero-pressure constraint (equations (A1) and (A2), respectively). The MDL decomposition results obtained by using either solely pressure field data or solely vertical-component particle velocity data are presented in Fig. 15 and 16, respectively.

Since we have applied specific notch filters to each of the two data sets, certain frequencies are missing in the resulting

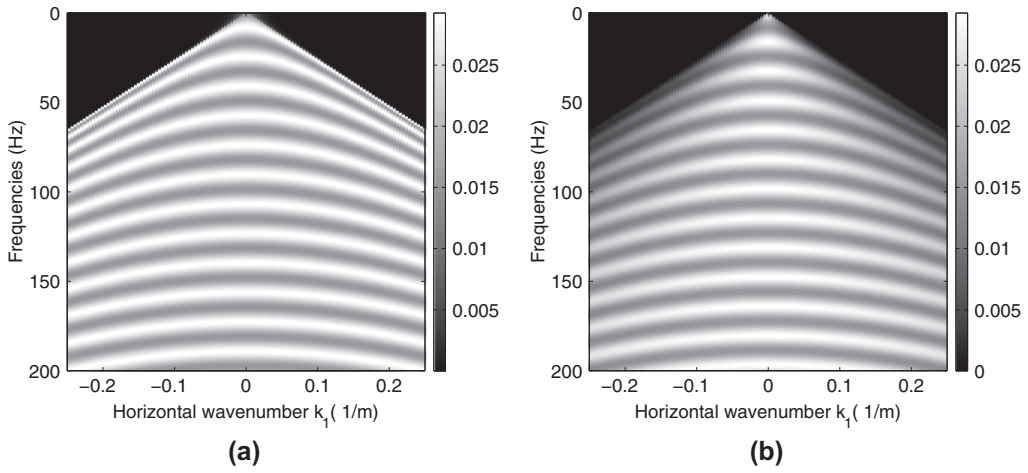

Figure 13 Wavenumber–frequency domain plots indicating the invertibility of the matrices $\tilde{\mathbf{S}}_p$ and $\tilde{\mathbf{S}}_{v_3}$. The plots show the inverse of the condition numbers for (**a**) the pressure field data, and (**b**) the vertical-component particle velocity data.

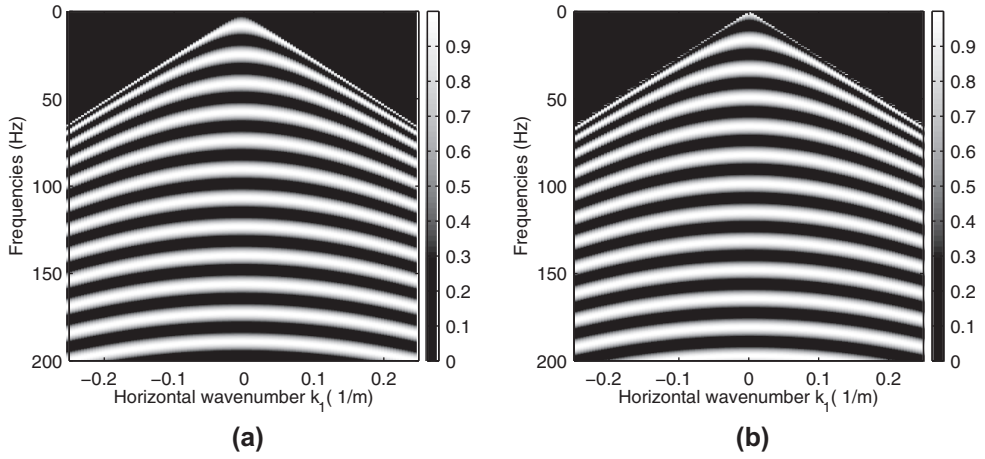

Figure 14 Designed notch filters to deal with the notch frequencies and hence overcoming the invertibility issues of $\tilde{\mathbf{S}}_p$ and $\tilde{\mathbf{S}}_{v_3}$. (**a**) Notch filter for the pressure field data. (**b**) Notch filter for the vertical-component particle velocity data.

decomposed data. Which frequencies are missing depends on which data set is used for the decomposition. However, since the pressure field data and particle velocity field data are complementary to each other, combining them will result again in full-frequency spectrum decomposed fields. Combining these two data sets can be performed at various stages. A straightforward way of combining pressure and particle velocity data is to add them. This addition can be designed in any desired way. One can for example normalize the two data sets by the norm of the energy of each data set, before adding them up. The underlying assumption is then that the total energy in the two data sets should be identical. The result of this addition is shown in Fig. 17. Comparing Fig. 15, 16 and 17 with the MC or MC-MDL results of Fig. 12, again shows that similar results can be obtained by using only pressure or vertical-component particle velocity data.

Despite the drawback of the notches, the introduced independence between the pressure and vertical-component particle velocity recordings has an additional benefit. As is well known for field data, differently recorded field quantities can have different receiver signatures superimposed. Each receiver modifies the recorded field via a specific transfer function when converting it to a voltage (El Allouche 2011). Since we can treat certain field quantities separately in the MDL decomposition scheme ($\tilde{p}$ and $\tilde{v}_z$ for the acoustic case), a compensation for these sensor characteristics is not required. The same transfer functions act on both the upgoing and downgoing fields.

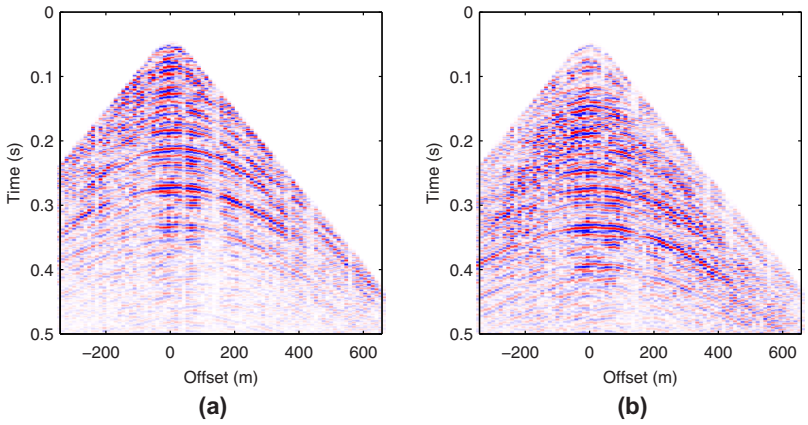

Figure 15 MDL decomposition results of the Annerveen data set using only pressure recordings at $x_{3;B}$ combined with a free-surface, zero-pressure constraint and after applying the designed notch filter. (**a**) MDL upgoing fields using only pressure field data and a free-surface zero-pressure constraint. (**b**) MDL downgoing fields using only pressure field data and a free-surface zero-pressure constraint.

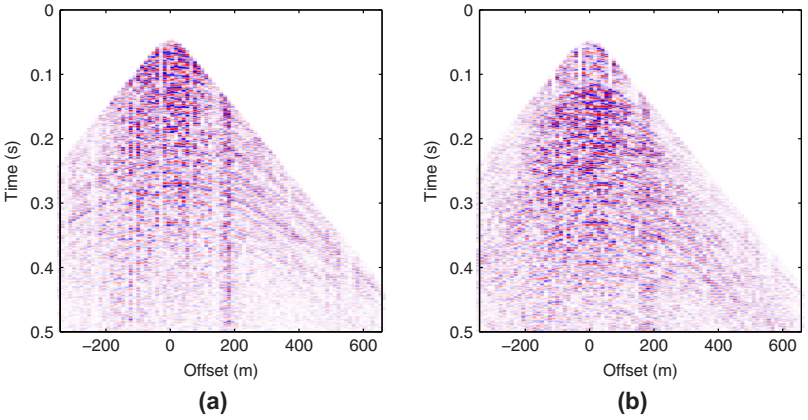

Figure 16 MDL decomposition results of the Annerveen data set using only vertical-component particle velocity data at $x_{3;B}$ combined with a free-surface, zero-pressure constraint and after applying the designed notch filter. (**a**) MDL upgoing fields using only vertical-component particle velocity field data and a free-surface zero-pressure constraint. (**b**) MDL downgoing fields using only vertical-component particle velocity data and a free-surface zero-pressure constraint.

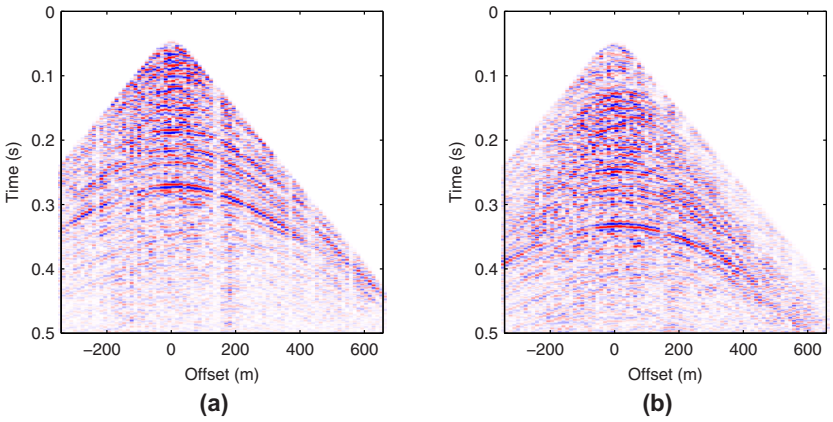

Figure 17 Summed MDL decomposition results of the Annerveen data set using only pressure recordings at $x_{3;B}$ or vertical-component particle velocity recordings at $x_{3;B}$. (**a**) Upgoing fields, by summing Figures 15(a) and 16(a). (**b**) Downgoing fields, by summing Figures 15(b) and 16(b).

APPENDIX B

ELECTROMAGNETIC FIELD DECOMPOSITION

We start by capturing the electromagnetic problem in the format of equation (1). When considering a medium that is invariant in two directions, it can be useful to decouple the total 3D system into two independent electromagnetic propagation modes: the transverse electric (TE) mode and the transverse magnetic (TM) mode, resulting in mode field vectors (Nabighian 1987). In 2D (when defining line sources in the crossline (x_2-) direction), the mode separation occurs

naturally. Since the eigenvectors of the full electromagnetic system in laterally invariant media are well known (Slob 2009), we here skip the theory of mode separation and directly describe how to apply the multi-depth level (MDL) field decomposition scheme to arbitrary subsurface geometries, just like the acoustic and elastodynamic systems treated in this paper.

Following Slob (2009), we might define the electromagnetic field vector $\tilde{\mathbf{q}}$ in this case as:

$$\tilde{\mathbf{q}} = \begin{pmatrix} \tilde{\mathbf{q}}_1 \\ \tilde{\mathbf{q}}_2 \end{pmatrix} = \begin{pmatrix} \tilde{E}_1 \\ \tilde{E}_2 \\ \tilde{H}_2 \\ -\tilde{H}_1 \end{pmatrix}. \tag{B1}$$

The whole electromagnetic system is described if we know four out of the six existing electromagnetic field quantities ($\tilde{E}_i$ and $\tilde{H}_i$). Recordings in a horizontal borehole result in recordings on a 'line'. Let us take the x_1-direction as the direction of our borehole, and refer to this direction as the inline direction. Not all components of the electric field can be measured in a borehole. In the above described case, only the inline electric field ($\tilde{E}_1$) can be measured in the borehole. Using coils, we can additionally measure

$$j\omega\tilde{B}_3 = -\tilde{E}^H = j\omega\mu_0\mu_R\tilde{H}_3 \tag{B2}$$

$$j\omega\tilde{B}_\alpha = j\omega\mu_0\mu_R\tilde{H}_\alpha, \tag{B3}$$

where the subscript α can take the values 1 and 2. Here, $\tilde{B}_k$ (with k =1,2 or 3) denotes the different field components of the averaged magnetic flux density. The coils can directly measure the time derivative of these magnetic flux densities. In addition for Earth materials, the relative magnetic permeability $\mu_R \approx 1$, and the magnetic permeability for vacuum μ_0 is a known constant. The quantity $\tilde{E}^H$ denotes the TE mode gradient of the electric field, which can be composed from the rotation of the horizontal-component electric field quantities $\tilde{E}_1$ and $\tilde{E}_2$ via

$$\tilde{E}^H = -jk_1\tilde{E}_2 + jk_2\tilde{E}_1. \tag{B4}$$

At depth, the TE mode gradient of the electric field is proportional to the vertical-component magnetic field $\tilde{H}_3$. We see that we can measure at least four components in an x_1-oriented borehole, where the magnetic fields are directly measured with coils and the electric fields ($\tilde{E}_1$) with electrodes. In the space–frequency domain, a few electrodes in the x_2-direction might be sufficient to measure the spatial derivative in the x_2-direction of the inline electric field in the x_1-direction (space–frequency version of equation (B4)). Since we also know $j\omega\hat{B}_3$ (space–frequency version of equation (B2)), we can calculate the derivative of $\hat{E}_2$ in the x_1-direction using the space–frequency versions of equations (B2) and (B4). Together with the space–frequency version of equation (B3), we have access to the required four electromagnetic components of our field vector. However, in the horizontal wavenumber–frequency domain, we encounter some practical issues. Suppose we can measure the spatial derivative of $\hat{E}_1$ in the x_2-direction. Transforming this field to the horizontal wavenumber–frequency domain to determine $jk_2\tilde{E}_1$ requires much more spatial measurements in the x_2-direction. This is practically impossible since we typically only have one borehole with limited borehole size in the x_2-direction. Hence, for an x_1-oriented borehole, we can only transform to the k_1-domain. Equation (B4) shows that we then need to measure $\tilde{E}_2$, which is practically also impossible due to limited borehole size in this direction.

The system can still be solved in the horizontal wavenumber–frequency domain, in case of a purely 2D situation. In this case, mode separation occurs naturally. The TE-mode field vector then reads

$$\tilde{\mathbf{q}}^H = \begin{pmatrix} \tilde{q}_1^H \\ \tilde{q}_2^H \end{pmatrix} = \begin{pmatrix} \tilde{E}_2 \\ -\tilde{H}_1 \end{pmatrix}, \tag{B5}$$

and the TM-mode field vector consists of

$$\tilde{\mathbf{q}}^V = \begin{pmatrix} \tilde{q}_1^V \\ \tilde{q}_2^V \end{pmatrix} = \begin{pmatrix} \tilde{E}_1 \\ \tilde{H}_2 \end{pmatrix}, \tag{B6}$$

Now, no gradients are required to obtain the necessary fields. When we have an acquisition geometry where the sources are located directly above an x_1-oriented borehole, $\tilde{E}_2$ and $\tilde{H}_1$ are zero in the (x_1, x_3) plane, leaving us with only a TM-mode electromagnetic system, which is the desired mode in electromagnetic acquisition for hydrocarbon exploration.

When using these 2D field vectors for the MDL decomposition, it can be easily seen that sufficient field quantities are measurable to carry out field decomposition. The composition matrix $\tilde{\mathbf{L}}$ belonging to these 2D field vectors can be easily derived from the 3D version as presented in Slob 2009. The MDL theory in this paper was presented in the horizontal wavenumber–frequency domain. When rewriting the system in terms of operators, the same MDL scheme can be applied in the space–frequency domain for laterally varying media at the level of decomposition. An example of how to apply these spatial operators for the electromagnetic case can be found in Van Stralen (1997).

From the presented MDL decomposition scheme, we know that we either need to measure $\tilde{\mathbf{q}}_1$ or $\tilde{\mathbf{q}}_2$. Depending on the acquisition geometry, we either look at MDL recordings

or a single-level recording combined with free-surface constraints. None of the presented field quantities in either $\tilde{\mathbf{q}}_1^{H,V}$ or $\tilde{\mathbf{q}}_2^{H,V}$ have a zero-value free-surface boundary constraint. Hence, in order to apply the MDL decomposition scheme to electromagnetic phenomena, we need recordings at at least two depth levels. Whether the borehole is fluid filled or whether the receivers are buried in the subsurface does not make a difference for the electromagnetic case since all tangential field components are continuous at a horizontal fluid-solid interface (Nabighian 1987, reprint 2008). However, the borehole wall should be non-metallic.

APPENDIX C

ELASTODYNAMIC FIELD DECOMPOSITION

In the elastodynamic case, we organize the two-way field vector as follows:

$$\tilde{\mathbf{q}} = \begin{pmatrix} \tilde{\mathbf{q}}_1 \\ \tilde{\mathbf{q}}_2 \end{pmatrix} = \begin{pmatrix} -\tilde{\tau}_{13} \\ -\tilde{\tau}_{23} \\ -\tilde{\tau}_{33} \\ \tilde{v}_1 \\ \tilde{v}_2 \\ \tilde{v}_3 \end{pmatrix}. \tag{C1}$$

Hence, $\tilde{\mathbf{q}}_1 = -\tilde{\boldsymbol{\tau}}_3$, and $\tilde{\mathbf{q}}_2 = \tilde{\mathbf{v}}$. Since the eigenvectors for arbitrary, laterally invariant subsurface geometries are well known for the elastodynamic system, we will here not consider the mode separation in independent SH and P-SV propagation modes. Our synthetic elastodynamic examples were based on 2D modelling. In this case, all x_2-directed field quantities in $\tilde{\mathbf{q}}$ and corresponding eigenvector elements in $\tilde{\mathbf{L}}$ decouple (and do not exist in our 2D example). In equation (C1), we have organized the field quantities in such a way that the field quantities that are likely to be measured (the particle velocity in $\tilde{\mathbf{q}}_2$) are separated from the ones that are unlikely to be measured (traction components acting on a horizontal plane in $\tilde{\mathbf{q}}_1$). Alternatively, we can organize the field quantities in such a way that the system matrix $\tilde{\mathbf{A}}$ obtains an anti-blockdiagonal symmetry for isotropic media (Ursin 1983):

$$\tilde{\mathbf{q}} = \begin{pmatrix} \tilde{\mathbf{q}}_1 \\ \tilde{\mathbf{q}}_2 \end{pmatrix} = \begin{pmatrix} \tilde{v}_3 \\ -\tilde{\tau}_{13} \\ -\tilde{\tau}_{23} \\ -\tilde{\tau}_{33} \\ \tilde{v}_1 \\ \tilde{v}_2 \end{pmatrix}. \tag{C2}$$

Once the eigenvectors are known for a certain field vector ordering (e.g., in equation (C1)), one can easily reorganize the field quantities and eigenvector matrix elements using permutation matrices (Wapenaar and Berkhout 1989).

For laterally varying media at the level of decomposition, all expressions need to be evaluated in the space–frequency domain and the use of pseudo-differential operators is required. An example of how to properly use these operators is given in e.g., Grimbergen *et al.* 1998; or Wapenaar *et al.* 2008, for a 3D acoustic and electromagnetic case, with 2D numerical examples. Elastodynamically, the derivation becomes already much more tedious (Wapenaar and Grimbergen 1996). In addition, coding everything numerically correct in the space–frequency domain might introduce new challenges. In the space–frequency domain, we need to be able to determine the derivative in the x_2-direction (when considering a borehole in the x_1-direction), just like for the electromagnetic case discussed previously. Also for pseudo-differential operators, a two-point measurement might not be sufficient to determine these derivatives. Therefore, multiple parallel boreholes (x_1-oriented boreholes parallel in the x_2-direction) might be required. A high density of vertical boreholes (e.g., Bakulin *et al.* 2012a, b), might be of use here as well. A practical solution might be to assume the medium is purely 2D and hence has no variations in the x_2-direction.

APPENDIX D

SEISMOELECTRIC AND POROELASTIC FIELD DECOMPOSITION

Seismoelectric phenomena deal with the coupling that occurs between seismic and electromagnetic fields, when those fields propagate through a fluid-filled porous medium. The governing equations as derived by Pride (1994), show that this complex physical phenomenon can be described by Biot's poroelasticity equations coupled to Maxwell's electromagnetic equations via a coupling coefficient $\hat{\mathcal{L}}$. The theory as derived by Pride (1994) holds for fluid-saturated porous media, which we will focus on in this appendix. Recently, the theory has been extended to partially saturated porous media (Warden *et al.* 2013). Since the necessary changes for this extension do not directly affect the eigenvectors of the seismoelectric system, the theory as presented in this appendix can still be applied.

One can capture the seismoelectric phenomenon in the format of equation (1) (Haartsen and Pride 1997). When considering a medium that is invariant in two directions, the total system can be separated into two independent propagation modes SH-TE and P-SV-TM. In 2D, this mode separation occurs naturally. The full, mode-coupled

eigenvector sets of the seismoelectric system for any arbitrary subsurface geometry are not known yet. We here focus on the known eigenvectors for the mode separated seismoelectric system (Pride and Haartsen 1996; Haartsen and Pride 1997; Grobbe and Slob 2013). In the SH-TE mode, the horizontally polarized shear waves are coupled to the transverse electric (TE) fields, whereas in the P-SV-TM propagation mode the pressure waves (fast and slow) are coupled to the transverse magnetic (TM) fields via the vertically polarized shear waves. Here, P_{fast} describes the fast compressional wave (the P-wave in the elastodynamic system), and P_{slow} describes the diffusive Biot slow compressional field (associated with an out-of-phase pore-fluid movement compared with the porous material; Kelder 1998).

Starting with equation (2), the field vector $\tilde{\mathbf{q}}$ can be organized in different ways. We can follow the field quantity ordering as presented by Haartsen and Pride (1997). Alternatively, we here follow the system as used by Grobbe and Slob (2013). The two main differences with the scheme of Haartsen and Pride (1997) are that Grobbe and Slob (2013) have power-flux-normalized their derived eigenvectors and have adjusted the system to correctly model situations where the seismoelectric coupling coefficient is set to zero (i.e., when the poroelastic system decouples from the electromagnetic system). In addition, Grobbe and Slob (2013) have used an opposite definition of the Fourier transform (the same one as is used in this paper) compared with Haartsen and Pride (1997), and they have used particle velocity field vectors instead of displacement vectors.

We can treat the two modes separately in equations (1) and (2). The field vectors for both the SH-TE (superscript H) and P-SV-TM (superscript V) modes then read

$$\tilde{\mathbf{q}}^H = \begin{pmatrix} \tilde{\mathbf{q}}_1^H \\ \tilde{\mathbf{q}}_2^H \end{pmatrix} = \begin{pmatrix} \tilde{v}_{norm}^{s,H} \\ \tilde{E}_{norm}^{H} \\ \tilde{\tau}_{norm}^{b,H} \\ -\tilde{H}_{norm}^{H} \end{pmatrix} \tag{D1}$$

and

$$\tilde{\mathbf{q}}^V = \begin{pmatrix} \tilde{\mathbf{q}}_1^V \\ \tilde{\mathbf{q}}_2^V \end{pmatrix} = \begin{pmatrix} \tilde{v}_3^s \\ \tilde{w}_3 \\ \tilde{\tau}_{norm}^{b,V} \\ \tilde{H}_{norm}^{V} \\ \tilde{\tau}_{33}^{b} \\ -\tilde{p}^f \\ \tilde{v}_{norm}^{s,V} \\ \tilde{E}_{norm}^{V} \end{pmatrix}. \tag{D2}$$

The superscript (H or V) indicates that certain field quantities are mode quantities. This means that the two modes need to be combined in 3D to obtain the true physical field quantities. We have normalized the field quantities of the SH-TE and P-SV-TM mode with a factor $-j\kappa$, such that, at the left-hand side and right-hand side of the equation, the same physical quantities are written. The different mode quantities are then defined as follows:

$$\tilde{v}_{norm}^{s,H} = \frac{k_1}{\kappa}\tilde{v}_2^s - \frac{k_2}{\kappa}\tilde{v}_1^s \tag{D3}$$

$$\tilde{\tau}_{norm}^{b,H} = \frac{k_1}{\kappa}\tilde{\tau}_{23}^b - \frac{k_2}{\kappa}\tilde{\tau}_{13}^b \tag{D4}$$

$$\tilde{E}_{norm}^{H} = \frac{k_1}{\kappa}\tilde{E}_2 - \frac{k_2}{\kappa}\tilde{E}_1 \tag{D5}$$

$$\tilde{H}_{norm}^{H} = \frac{k_1}{\kappa}\tilde{H}_1 + \frac{k_2}{\kappa}\tilde{H}_2 \tag{D6}$$

$$\tilde{v}_{norm}^{s,V} = \frac{k_1}{\kappa}\tilde{v}_1^s + \frac{k_2}{\kappa}\tilde{v}_2^s \tag{D7}$$

$$\tilde{\tau}_{norm}^{b,V} = \frac{k_1}{\kappa}\tilde{\tau}_{13}^b + \frac{k_2}{\kappa}\tilde{\tau}_{23}^b \tag{D8}$$

$$\tilde{E}_{norm}^{V} = \frac{k_1}{\kappa}\tilde{E}_1 + \frac{k_2}{\kappa}\tilde{E}_2 \tag{D9}$$

$$\tilde{H}_{norm}^{V} = \frac{k_1}{\kappa}\tilde{H}_2 - \frac{k_2}{\kappa}\tilde{H}_1. \tag{D10}$$

This normalization additionally aims to obtain a certain symmetry in the P-SV-TM system matrix $\tilde{\mathbf{A}}^V$ that helps to determine the power-flux-normalized eigenvectors of the composition matrix $\tilde{\mathbf{L}}^V$. In the above, $\tilde{v}_i^s$ (with $i = 1,2$ or 3) denotes the phase-averaged solid particle velocity field components, $\tilde{w}_3$ the vertical-component of the Biot filtration velocity, $\tilde{p}^f$ the phase-averaged fluid pressure, $\tilde{\tau}_{i3}^b$ the bulk-averaged stress components in the x_3-direction, and $\tilde{E}_\alpha$ and $\tilde{H}_\alpha$ the horizontal components of the electric field and magnetic field, respectively (with $\alpha = 1$ or 2).

We know that for multi-component (MC) field decomposition, all field quantities in $\tilde{\mathbf{q}}$ must be measured. For seismoelectrics, a huge amount of field quantities needs to be measured. In reality, not all field quantities can be measured (e.g., certain stress field components or the filtration velocity are not measurable). They also might be obscured by different sensor characteristics or noise levels. Finally, requiring to measure many different quantities in the field makes the operation financially and practically unfavourable.

From equations (28) and (29), we know that the MDL scheme is customizable. We can select those field quantities that are easily measurable in reality or that are well-defined by certain boundary conditions. We thereby need to take care that the customized composition matrix is of sufficient rank and notch problems are properly taken care of.

We focus on a single horizontal sensor array at depth levels $x_{3;B}$, and $x_{3;A}$ coinciding with the free surface. If we make use of the dynamic boundary conditions (Aki and Richards 1980), this implies that all stress components go to zero at the free surface: $\tilde{\tau}^{b;H,V} = 0$, and $\tilde{p}^f = 0$. Constraining the stress implies that the particle velocity fields (kinematic boundary conditions) are then 'free' variables. In addition, at the free surface, continuity of the horizontal components of the electromagnetic field quantities holds. We can carry out multi-depth level (MDL) decomposition by having measurements of either $\tilde{\mathbf{q}}_1$ or $\tilde{\mathbf{q}}_2$ at $x_{3;B}$, with the field quantity subvector at $x_{3;A}$ being equal to zero. In the case of the SH-TE system, this means that we need at least two field quantities equal to zero and have two measured quantities. For the P-SV-TM system, we need four field quantities equal to zero and four measured quantities.

For controlled-source electromagnetics (CSEM), the TM-mode magnetic field $\tilde{H}^V$ can be taken zero at the Earth's surface under the diffusive field approximation (Nabighian 1987). Looking at the P-SV-TM system, we can now see that we have four quantities that are zero at the free surface (the stress quantities, pore-fluid pressure, and the P-SV-TM mode magnetic field). At the measurement level $x_{3;B}$, we then need to select four quantities that we can measure, for example $\tilde{v}_3^s$, $\tilde{E}^V_{norm}$, $\tilde{p}^f$, $\tilde{H}^V_{norm}$, or $\tilde{v}^{s,V}_{norm}$. Two of those quantities are directly measurable in the borehole $\tilde{v}_3^s$ and $\tilde{p}^f$. From the electromagnetic scenario, we concluded that, due to limited borehole dimensions, we can only transform to the k_1-domain (for an x_1-oriented borehole). Therefore, all combined mode quantities in the horizontal wavenumber–frequency domain are hard to obtain since they all require an additional transformation to the k_2-domain. A difference between the mode electric fields and for example the mode particle velocity fields is that the $\tilde{E}_2$ component is additionally not measurable in an x_1-directed borehole due to the limited borehole size, whereas both the $\tilde{v}_1^s$ and $\tilde{v}_2^s$ particle velocity components are measurable.

When we carry out the field decomposition in the space–frequency domain, we can determine the spatial derivatives with respect to the x_1-direction and possibly also with respect to the x_2-direction. We can then obtain the four required field quantities to carry out the MDL decomposition: $\hat{v}_3^s$ and $\hat{p}^f$ and $\hat{v}^{s,V}_{norm}$ and $\hat{H}^V_{norm}$. However, for this we need to be able to derive correct pseudo-differential operators, which will be extremely tedious for this complex physical phenomenon.

It is good to be aware that certain seismoelectric source–receiver combinations (e.g., looking at a horizontal electric field in the x_1-direction $\tilde{E}_1$ due to a vertical seismic bulk force source $\tilde{f}_3^b$) are purely described by the P-SV-TM propagation mode (Grobbe and Slob 2013). Hence, for these recorded source–receiver combinations, MDL decomposition according to the P-SV-TM mode only is sufficient.

For the SH-TE case, we see that only the stress field $\tilde{\tau}^{b,H}$ is zero at the free surface. The second required quantity at $x_{3;A}$ should then be measured. Therefore, we can place for example a vertical magnetic coil at the free surface and measure $\tilde{E}^H$. Combining surface and buried measurements is, for practical purposes, not so attractive since surface measurements suffer too much from low fidelity, significant noise (e.g., surface waves or power line noise), and low repeatability. However, when $x_{3;A}$ coincides with the Earth's surface, we are for our measurements not limited in any horizontal spatial direction. At depth level $x_{3;B}$, we can then select two field quantities we would like to measure to solve the MDL decomposition problem for the SH-TE mode. Since $\tilde{E}^H$ is directly measurable (equation (B2)), this is a logical choice. However, when trying to obtain the mode quantities $\tilde{H}^H$ and $\tilde{v}^H$, the same issues are encountered as discussed above for the P-SV-TM case. Luckily, as discussed in the other appendices, we can still solve the seismoelectric MDL decomposition problem in the horizontal wavenumber–frequency domain in case of a purely 2D situation.

When we look at the dual depth horizontal sensor arrays, we can select the desired measurable field quantities for each mode at both depth levels $x_{3;A}$ and $x_{3;B}$ and adjust the composition matrix $\tilde{\mathbf{S}}$ accordingly. The issues in obtaining certain field quantities due to limited borehole size now play a role at both depth levels.

Sometimes the mode splitting into SH-TE and P-SV-TM propagation modes might not be useful or even not applicable, e.g., when we are considering anisotropic media or in non-layered Earth systems. Alternatively, we can take the field vector as defined in Wapenaar and Fokkema (2004), where all physical field quantities are directly present. However, this system is probably redundant, and the decomposition problem might be solvable with less field quantities (comparable to the electromagnetic case of Appendix B). Theoretically, we can describe the field decomposition starting from equation (2). However, the composition matrix $\tilde{\mathbf{L}}$ consisting of the eigenvectors of the full non-mode separated system of

seismoelectric equations is not yet derived. Furthermore, the equations should be explicitly extended for anisotropic media. Nevertheless, if we assume that we know the corresponding eigenvectors of the system of equations, we can select desired measured field quantities and carry out MDL decomposition according to the presented scheme. In this case, we do not suffer from separate modes and mode quantities that need to be combined via spatial derivatives and hence not from issues when transforming to the horizontal wavenumber–frequency domain.

The poroelastic system can be considered a special case of the seismoelectric system. If the seismoelectric coupling coefficient $\hat{\mathcal{L}}$ is equal to zero there is no coupling between the poroelastic system and the electromagnetic system. In this case, we can treat the electromagnetic system and the poroelastic system separately (Grobbe *et al.* 2014).

We can obtain the mode-separated poroelastic field vectors directly from the seismoelectric field vectors by omitting the electromagnetic field quantities from equations (D1) and (D2) and keeping the order of the mechanical field quantities the same.

So, starting from the seismoelectric eigenvectors used by Grobbe and Slob (2013), removing the columns belonging to the TE and TM mode electromagnetic fields and putting the coupling coefficient to zero results in the poroelastic eigenvectors corresponding to this poroelastic field vector ordering. Alternatively, Jocker *et al.* (2004) derived and presented the poroelastic eigenvectors for a 2D scenario. As discussed earlier, when we have line recordings in a borehole, this results effectively in a 2.5D or 2D scenario. For the 2.5D scenario, we again encounter the same issues in obtaining the mode quantities due to the limited size of a borehole. In 2D, the mode separation in SH and P-SV modes occurs naturally, assuming line sources in the x_2-direction. In 2D, the MDL decomposition problem can straightforwardly be solved similar to the scenarios discussed for seismoelectric fields.

Alternatively to mode separation, the full poroelastic system and corresponding eigenvectors for arbitrary subsurface geometries can be used. However, to our knowledge, the eigenvector system forming the composition matrix for 3D poroelastic fields is not yet published. If these eigenvectors are known, we can select desired measured field quantities. Measurements of four field quantities, e.g., three-component particle velocity recordings in combination with pore fluid pressure measurements, would be sufficient to solve the MDL decomposition problem for poroelastic fields.

REFERENCES

Aki K. and Richards P.G. 1980. *Quantitative Seismology*. Freeman and Company, New York.

Alexandrov D., Bakulin A. and Burnstad R. 2012. Redatuming of synthetic land data with shallow buried receivers using the virtual source method. *82nd SEG meeting*, Las Vegas, USA, Expanded Abstracts, 1–5.

Alexandrov D., Bakulin A., Leger P. and Kashtan B. 2014. Dual-sensor summation with buried land sensors. *84th SEG meeting*, Denver, USA, Expanded Abstracts, 1929–1933.

Almagro Vidal C. and Wapenaar K. 2014. Passive seismic interferometry by multi-dimensional deconvolution-decorrelation. *84th SEG meeting*, Denver, USA, Expanded Abstracts, 2224–2228.

Almagro Vidal C., van der Neut J., Draganov D., Drijkoningen G. and Wapenaar K. 2011. Retrieval of reflections from ambient-noise field data using illumination diagnostics. *81st SEG meeting*, San Antonio, USA, Expanded Abstracts, 1613–1617.

Almagro Vidal, C., Draganov D., Van der Neut J., Drijkoningen G., and Wapenaar K., 2014. Retrieval of reflections from ambient noise using illumination diagnosis, *Geophysical Journal International*, **198**, 1572–1584.

Amundsen L. 1999. Elimination of free surface-related multiples without need of the source wavelet. *69th SEG meeting*, Houston, USA, Expanded Abstracts, 1064–1067.

Amundsen L. and Holvik E. 2004. *Processing Electromagnetic Data*. Patent GB2415511.

Amundsen L., Lóseth L., Mittet R., Ellingsrud S. and Ursin B. 2006. Decomposition of electromagnetic fields into upgoing and downgoing components. *Geophysics* **71**(5), G211–G223.

Amundsen L. and Reitan A. 1995. Decomposition of multicomponent sea-floor data into upgoing and downgoing P- and S-waves. *Geophysics* **60**, 563–572.

Amundsen L. and Robertsson J.O.A. 2014. Wave equation processing using finite-difference propagators part 1: Wavefield dissection and imaging of marine multicomponent seismic data, *Geophysics* **79**(6), T287–T300.

Bakulin A., Burnstad R., Jervis M. and Kelamis P. 2012a. The feasibility of permanent land seismic monitoring with buried geophones and hydrophones in a desert environment. *74th EAGE Conference & Exhibition*, Copenhagen, Denmark, 1–5.

Bakulin A., Burnstad R., Jervis M. and Kelamis P. 2012b. Evaluating permanent seismic monitoring with shallow buried sensors in a desert environment. *82nd SEG meeting*, Las Vegas, USA, Expanded Abstracts 1–5.

Bakulin A. and Calvert R., 2006. The virtual source method: theory and case study. *Geophysics* **71**(4), SI139–SI150.

Beasley C.J., Coates R., Ji Y. and Perdomo J. 2013a. Wave equation receiver dehosting: a provocative example, *83rd SEG meeting*, Houston, USA, Expanded Abstracts, 4226–4230.

Beasley C.J., Coates R. and Lapilli C. 2013b. Wave equation receiver deghosting. *IEEE 5th International Workshop on Computational Advances in Multi-Sensor Adaptive Processing*, St. Martin, France, 280–283.

Berron C., Forgues E., Jervis M., Bakulin A. and Burnstad R. 2012. Buried sources and receivers in a karsted desert environment.

74th EAGE Conference & Exhibition, Copenhagen, Denmark, 1–5.

Bleistein N., 1987. On the imaging of reflectors in the earth. *Geophysics* **52**, 931–942.

Bleistein N., Cohen J.K. and Hagin F.G., 1987. Two and one-half dimensional born inversion with an arbitrary reference. *Geophysics* **52**, 26–36.

Burnstad R., Bakulin A., Jervis M. and Alexandrov D. 2012. Successful imaging of land hydrophone and dual sensor data in a dry desert environment. *82nd SEG meeting*, Las Vegas, USA, Expanded Abstracts, 1–5.

Cheng C.H. and Toksöz M.N. 1981. Elastic wave propagation in a fluid-filled borehole and synthetic acoustic logs. *Geophysics* **46**, 1042–1053.

Cotton J. and Forgues E. 2012. Dual-depth hydrophones for ghost reduction in 4D land monitoring. *82nd SEG meeting*, Las Vegas, USA, Expanded Abstracts, 1–5.

Dankbaar J.W.M., 1985. Separation of P- and S-waves. *Geophysical Prospecting* **33**, 970–986.

Day A., Klüver, T., Söllner W., Hocine T. and Carlson D., 2013. Wavefield-separation methods for dual-sensor towed-streamer data. *Geophysics* **78**(2), WA55–WA70.

Draganov D., Wapenaar K. and Thorbecke J., 2006. Seismic interferometry: reconstructing the earth's reflection response. *Geophysics* **71**(4), SI61–SI70.

El Allouche N. 2011. Converted waves in shallow marine environments: modelling and field experiments. *Ph.D. thesis*, Delft University of Technology, Netherlands.

Fishman L., McCoy J.J. and Wales S.C., 1987. Factorization and path integration of the Helmholtz equation: Numerical algorithms. *Journal of the Acoustical Society of America* **81**, 1355–1376.

Fokkema J.T. and Van den Berg P.M. 1993. *Seismic Applications of Acoustic Reciprocity*. Elsevier Science Publishers B.V.

Frasier C.W., 1970. Discrete time solution of plane P-SV waves in a plane layered medium. *Geophysics* **35**, 197–219.

Frijlink M. and Wapenaar K., 2010. Reciprocity theorems for one-way wave fields in curvilinear coordinate systems. *SIAM Journal on Imaging Sciences* **3**, 390–415.

Frijlink M., Van Borselen R. and Söellner W., 2011. The free surface assumption for marine data-driven demultiple methods. *Geophysical Prospecting* **59**, 269–278.

Grimbergen J.L.T., Dessing F.J. and Wapenaar K., 1998. Modal expansion of one-way operators in laterally varying media. *Geophysics* **63**, 995–1005.

Grobbe N. and Slob E. 2013. Validation of an electroseismic and seismoelectric modeling code for layered earth models, by the explicit homogeneous space solutions. *83rd SEG meeting*, Houston, USA, Expanded Abstracts, 1847–1851.

Grobbe N., Van der Neut J., Almagro Vidal C., Drijkoningen G. and Wapenaar K. 2014. Wavefield decomposition of field data, using a shallow horizontal downhole sensor array and a free-surface constraint. *76th EAGE Conference & Exhibition*, Amsterdam, Netherlands, 1–5.

Haartsen M.W. and Pride S.R., 1997. Electroseismic waves from point sources in layered media. *Journal of Geophysical Research* **102**(B11), 24745–24769.

Holvik E. and Amundsen L., 2005. Elimination of the overburden response from multicomponent source and receiver seismic data, with source designature and decomposition into PP-, PS-, SP-, and SS-wave responses. *Geophysics* **70**(2), S43–S59.

Jocker J., Smeulders D., Drijkoningen G., Van der Lee C. and Kalfsbeek A. 2004. Matrix propagator method for layered porous media: Analytical expressions and stability criteria. *Geophysics* **69**, 1071–1081.

Kelder O. 1998. Frequency-dependent wave propagation in water-saturated porous media. *PhD thesis*, Delft University of Technology, Netherlands.

Kennett B.L.N., 1983. *Seismic Wave Propagation in Stratified Media*. Cambridge University Press.

Majdanski M., Kostov C., Kragh E., Moore I., Thompson M. and Mispel J., 2011. Attenuation of free-surface multiples by up/down deconvolution for marine towed-streamer data. *Geophysics* **76**(6), V129–V138.

Maxwell S.C., Rutledge J., Jones R. and Fehler M. 2010. Petroleum reservoir characterization using downhole microseismic monitoring. *Geophysics* **75**(5), 75A129–75A137.

Mehta K., Bakulin A., Sheiman J., Calvert R. and Snieder R., 2007. Improving the virtual source method by wavefield separation. *Geophysics* **72**(4), V79–V86.

Moldoveanu N., Combee L., Egan M., Hampson G., Sydora L. and Abriel W., 2007. Over/under towed-streamer acquisition: A method to extend seismic bandwidth to both higher and lower frequencies. *The Leading Edge* **26**, 41–58.

Muijs R., Robertsson J.O. and Holliger K., 2007. Prestack depth migration of primary and surface-related multiple reflections part I: imaging. *Geophysics* **72**(2), S59–S69.

Nabighian M.N. 1987. *Electromagnetic Methods in Applied Geophysics*. Society of Exploration Geophysicists.

Nakata N., Snieder R. and Behm M., 2014. Body-wave interferometry using regional earthquakes with multidimensional deconvolution after wavefield decomposition at free surface. *Geophysical Journal International* **199**, 1125–1137.

Peng C., Cheng C.H. and Toksöz M.N., 2003. Borehole effects on downhole seismic measurements. *Geophysical Prospecting* **41**, 883–912.

Pride S., 1994. Governing equations for the coupled electromagnetics and acoustics of porous media. *Physical Review B* **50**(21), 15678–15696.

Pride S.R. and Haartsen M.W., 1996. Electroseismic wave properties. *Journal of the Acoustical Society of America* **100**, 1301–1315.

Robertsson J.O.A. and Amundsen L., 2014. Wave equation processing using finite-difference propagators, part 2: Deghosting of marine hydrophone seismic data. *Geophysics* **79**(6), T301–T312.

Schalkwijk K.M., Wapenaar C.P.A. and Verschuur D.J., 2003. Adaptive decomposition of multicomponent ocean-bottom seismic data into downgoing and upgoing P- and S-waves. *Geophysics* **68**, 1091–1102.

Slob E., 2009. Interferometry by deconvolution of multicomponent multioffset GPR data. *IEEE Transactions on Geoscience and Remote Sensing* **47**, 828–838.

Thorbecke J.W. and Draganov D., 2011. Finite-difference modeling experiments for seismic interferometry. *Geophysics* **76**(6), H1–H18.

Ursin B., 1983. Review of elastic and electromagnetic wave propagation in horizontally layered media. *Geophysics* **48**, 1063–1081.

Van Borselen R.G., Fokkema J. and Van den Berg P. 2013. Wavefield decomposition based on acoustic reciprocity: theory and applications to marine acquisition. *Geophysics* **78**(2), WA41–WA54.

Van der Neut J., Bakulin A. and Alexandrov D. 2013. Acoustic wavefield separation using horizontal receiver arrays deployed at multiple depth on land. *83rd SEG meeting*, Houston, USA, Expanded Abstracts, 4601–4607.

Van der Neut J., El Allouche N. and Wapenaar K. 2010. Elastic decomposition with downhole geophones and hydrophones. *80th SEG meeting*, Denver, USA, Expanded Abstracts, 1708–1713.

Van der Neut J. and Herrmann F.J. 2012. Up/down wavefield decomposition by sparse inversion. *74th EAGE Conference & Exhibition*, Copenhagen, Denmark, 4693–4698.

Van Stralen M.J.N. 1997. *Directional decomposition of electromagnetic and acoustic wave-Fields-applications in integrated optics, exploration seismics and underwater acoustics*. PhD Thesis, Delft University of Technology, Netherlands.

Virieux J., 1986. P-SV wave propagation in heterogeneous media: velocity-stress finite difference method. *Geophysics* **51**, 889–901.

Wapenaar C.P.A. and Berkhout A.J. 1989. *Elastic Wavefield Extrapolation – Redatuming of Single and Multi-Component Seismic Data*. Elsevier.

Wapenaar C.P.A., Dillen M.W.P. and Fokkema J.T. 2001. Reciprocity theorems for electromagnetic or acoustic one-way wave fields in dissipative inhomogeneous media. *Radio Science* **36**, 851–863.

Wapenaar C.P.A. and Grimbergen J.L.T., 1996. Reciprocity theorems for one-way wavefields. *Geophysical Journal International* **127**, 169–177.

Wapenaar C.P.A. and Verschuur D.J. 1996. Processing of Ocean Bottom Data: The Dolphin Project, Vol. **I**, pp. 6.1–6.26.

Wapenaar C.P.A., Herrmann P., Verschuur D.J. and Berkhout A.J., 1990. Decomposition of multi-component seismic data into primary P- and S-wave responses. *Geophysical Prospecting* **38**, 633–661.

Wapenaar K., 1998. Reciprocity properties of one-way propagators. *Geophysics* **63**, 1795–1798.

Wapenaar K. and Fokkema J., 2004. Reciprocity theorems for diffusion, flow and waves. *Journal of Applied Mechanics* **71**, 145–150.

Wapenaar K., Slob E. and Snieder R., 2008. Seismic and electromagnetic controlled-source interferometry in dissipative media. *Geophysical Prospecting* **56**, 419–434.

Wapenaar K., Van der Neut J., Ruigrok E., Draganov D., Hunziker J., Slob E. et al. 2011. Seismic interferometry by crosscorrelation and by multi-dimensional deconvolution: a systematic comparison. *Geophysical Journal International* **185**, 1335–1364.

Warden S., Garambois S., Jouniaux L., Brito D., Sailhac P. and Bordes C., 2013. Seismoelectric wave propagation numerical modelling in partially saturated materials. *Geophysical Journal International* **194**, 1498–1513.

White J.E. 1965. *Seismic Waves: Radiation, Transmission, and Attenuation*. McGraw-Hill, New York.

Woodhouse J.H., 1974. Surface waves in a laterally varying layered structure. *Geophysical Journal International* **37**(3), 461–490.

Xu Z., Juhlin C., Gudmundsson O., Zhang F., Yang C., Kashubin A. et al., 2012. Reconstruction of subsurface structure from ambient seismic noise: an example from Ketzin, Germany. *Geophysical Journal International* **189**, 1085–1102.